Range expansions transition from pulled to pushed waves as growth becomes more cooperative in an experimental microbial population

Range expansions transition from pulled to pushed waves as growth becomes more cooperative in an experimental microbial population

Saurabh R. Gandhi[a], Eugene Anatoly Yurtsev[a], Kirill S. Korolev[b,c,1], and Jeff Gore[a,1]

[a]Physics of Living Systems Group, Department of Physics, Massachusetts Institute of Technology, Cambridge, MA 02139; [b]Department of Physics, Boston University, Boston, MA 02215; and [c]Graduate Program in Bioinformatics, Boston University, Boston, MA 02215

Edited by Alan Hastings, University of California, Davis, CA, and approved April 22, 2016 (received for review October 27, 2015)

Range expansions are becoming more frequent due to environmental changes and rare long-distance dispersal, often facilitated by anthropogenic activities. Simple models in theoretical ecology explain many emergent properties of range expansions, such as a constant expansion velocity, in terms of organism-level properties such as growth and dispersal rates. Testing these quantitative predictions in natural populations is difficult because of large environmental variability. Here, we used a controlled microbial model system to study range expansions of populations with and without intraspecific cooperativity. For noncooperative growth, the expansion dynamics were dominated by population growth at the low-density front, which pulled the expansion forward. We found these expansions to be in close quantitative agreement with the classical theory of pulled waves by Fisher [Fisher RA (1937) *Ann Eugen* 7(4):355–369] and Skellam [Skellam JG (1951) *Biometrika* 38(1-2):196–218], suitably adapted to our experimental system. However, as cooperativity increased, the expansions transitioned to being pushed, that is, controlled by growth and dispersal in the bulk as well as in the front. Given the prevalence of cooperative growth in nature, understanding the effects of cooperativity is essential to managing invading species and understanding their evolution.

Allee effect | Fisher wave | biological invasion

From a local disturbance by an invasive species to the global expansion of the biosphere after an ice age, range expansions have been a major ecological and evolutionary force (1, 2). Range expansions and range shifts are becoming increasingly frequent due to the deliberate introduction of foreign species (3, 4), unintentional introductions caused by global shipping (5), and temperature changes associated with climate change (6, 7). Many invasions disturb ecosystem functions, reduce biodiversity, and impose significant economic costs (8, 9). The interest in invasion forecasting and management resulted in a substantial effort to develop predictive mathematical models of range expansions (4, 10–13), but empirical tests of these models have been less extensive.

Species invade new territory through a combination of dispersal and local growth. Mathematically, these dynamics can be described by a variety of models depending on the details of the species ecology or simplifying assumptions (14). For example, the invasion of house finches in North America has been successfully modeled with integrodifference equations (4). Continuous reaction–diffusion equations have been used to describe the expansion of trees following the end of an ice age and the expansion of muskrats from central Europe (15), whereas metapopulation models with disjoint patches of suitable habitat and discrete generations are more appropriate for certain butterflies living in temperate climates (16). One of the great achievements of mathematical ecology is the discovery that all these diverse models of population expansion can be divided into two broad classes of pulled and pushed expansions with very different properties.

The class of the expansion is determined by how the per capita growth rate depends on population density (17–19). Whereas some populations experience only intraspecific competition and grow best at very low densities, others exhibit an Allee effect and grow best at intermediate densities, due to intraspecific cooperation, higher chances of finding mates, or other factors (20–23). These Allee effects may be weak (reduced but positive growth rate at low density) or strong (inability to survive at low density). Pulled expansions occur when Allee effects are small, and the expansion velocity depends only on the growth rate at low densities and the rate of dispersal. Such expansions are dominated by the dynamics at the very edge of the expanding wave front, which effectively pulls the wave forward (17, 18, 24). As a result, pulled invasions are known to be sensitive to demographic fluctuations and lead to rapid loss of genetic diversity because the population size at the expansion edge is very small (25–29). When the Allee effect is more severe, including but not restricted to the case of strong Allee effects, the expansions are pushed. In contrast to the simple and universal theory of pulled expansions, the velocity and other properties of pushed expansions depend on the per capita growth rate at all population densities, and thus are sensitive to all of the details of the species ecology (17, 18, 24).

Because direct observations of the Allee effect are often challenging, it is important to find alternative ways to distinguish pulled and pushed expansions. Unfortunately, these two invasion classes share many generic properties. In particular, both expansions advance as population waves that move at constant velocity and maintain a constant shape of the expansion front. Even the qualitative shape of the expansion front is the same for pulled and pushed waves because population densities decay exponentially at the expansion edge in both cases (17, 18). Thus, one needs quantitative rather than qualitative comparison between theory and observations to distinguish pulled and pushed waves.

Significance

Species undergo range shifts in response to changing climate or following an introduction to a new environment. Invasions often incur significant economic cost and threaten biodiversity. Ecological theory predicts two distinct types of expansion waves, pulled and pushed, depending on the degree of cooperativity in the population. Although pulled and pushed invasions differ dramatically in how population-level properties such as the expansion rate depend on the organism-level properties such as rates of growth and dispersal, these theoretical predictions have not been tested empirically. Here, we use a microbial model system to perform these tests and demonstrate that pulled and pushed waves can be distinguished based on their dynamics.

Author contributions: S.R.G., E.A.Y., K.S.K., and J.G. designed research; S.R.G. performed research; S.R.G., E.A.Y., K.S.K., and J.G. analyzed data; and S.R.G., E.A.Y., K.S.K., and J.G. wrote the paper.

The authors declare no conflict of interest.

This article is a PNAS Direct Submission.

Freely available online through the PNAS open access option.

See Commentary on page 6819.

[1]To whom correspondence may be addressed. Email: korolev@bu.edu or gore@mit.edu.

This article contains supporting information online at www.pnas.org/lookup/suppl/doi:10.1073/pnas.1521056113/-/DCSupplemental.

Although high-quality quantitative data on range expansions is often limited, several studies have successfully tested theories of range expansions in natural and laboratory populations. Veit and Lewis (4) could accurately describe the spread of house finches in North America by incorporating an Allee effect and long-distance dispersal. Importantly, this was one of the early studies highlighting the difference between pulled and pushed invasions. Lewis and Kareiva (30) had earlier shown that the rate of spread also depends on the initial spatial abundance profile of the invader. Melbourne and Hastings (31) have carried out a very detailed comparison between theory and experiment for a laboratory population of flour beetles and showed that the unavoidable heterogeneity of the founding organisms leads to large variation in the rate of spread between replica populations. At the microscopic scale, Wakita et al. (32) tested the expected relation between the rate of spread and nutrient availability in *Escherichia coli*, and Giometto et al. (33) used the theory of pulled waves to describe the expansion of tetrahymena in linear channels. All of these studies, however, focused only on the rate of invasion and did not test theoretical predictions for the shape of the invading fronts. More importantly, these studies were conducted in a single environment and did not attempt to distinguish pulled and pushed expansions, in part because there was no experimental population that could undergo both pulled and pushed expansions.

Experimental microbial populations are a tractable system to study ecological phenomena without the overwhelming complexity of the natural world. However, such experiments can guide our thinking, show which theoretical predictions may be observable in nature (34, 35), and help develop new models (36). For example, range expansions of microbial populations have revealed the dependence of the invasion velocity on the supply of resources (37) and demographic stochasticity (33). Experiments with microbes have also demonstrated the strong effect of range expansion on competition (38–44) and neutral evolution via the founder effect or gene surfing (45, 46). In this study, we focus on expansions with and without the Allee effect and quantify their differences. Because it is possible to control and measure population sizes in microbial populations over a few orders of magnitude, our experimental system is particularly well-suited for studying the shape of the expansion fronts, as well as for future investigations on the rates of diversity loss and effects of habitat fragmentation such as invasion pinning (47, 48).

To recreate a range expansion in the laboratory, we used a metapopulation of budding yeast *Saccharomyces cerevisae*. Yeast grows best at low densities on simple sugars such as glucose or galactose but has a well-characterized Allee effect in the disaccharide sucrose (49–52). Sucrose is digested cooperatively because the yeast cells secrete an enzyme to hydrolyze extracellular sucrose into glucose and fructose, which are then transported into the cell. Higher cell densities facilitate the utilization of glucose, and therefore the growth rate of yeast on sucrose is maximum at intermediate population densities, where glucose utilization is high but competition is not yet strong. Importantly, the strength of the Allee effect can be controlled by tuning the relative concentrations of glucose and sucrose in the growth medium. Using this experimental system, we tested nontrivial properties of invasions including the exponential spatial decay of population density at the front. We then observed the transition from pulled to pushed expansion waves as the Allee effect was made more severe and found signatures of this transition in the expansion velocity and front shape. Our work confirms that Allee effects substantially affect invasion dynamics and demonstrates that pushed and pulled invasions can be distinguished by quantitative measurements.

Results

Experimental System. To study range expansions, we allowed the yeast populations to expand in one dimension along the columns of a 96-well plate. Each well represented a patch of suitable environment in a metapopulation where growth and death cycles occurred via a resupply of nutrients and dilution. Dispersal was achieved via exchange of small volumes of the growth media, corresponding to the migration rate (m), between the nearest wells (Fig. 1*A* and *SI Appendix*, Fig. S14). The experiments were started with a steep exponential initial population density profile, and after the profiles equilibrated over a few cycles we used flow cytometry to measure the density profiles of the emergent waves. This allowed us to measure with high accuracy the velocity (v) and the spatial decay rate of the exponential front (λ) over multiple orders of magnitude of population density (Fig. 1 *B* and *C*).

Range expansions of yeast in our metapopulations are well described by a simple model incorporating growth and nearest-neighbor dispersal. Assuming that an unconnected population starting at some density n grows to a final density given by $g_{\Delta t}(n)$ in one cycle of length Δt, the dynamics in connected populations, which have dispersal followed by growth, are given by

$$n_{t+\Delta t,x} = g_{\Delta t}\left(n_{t,x} + D_{eff}\frac{\Delta t}{\Delta x^2}\left(n_{t,x+\Delta x} + n_{t,x-\Delta x} - 2n_{t,x}\right)\right). \quad [1]$$

Here, t and x are time and position, Δt and Δx are time of the dilution cycles and separation between the wells, and D_{eff} is the dispersal rate determined by how much fluid is exchanged between the wells (see *SI Appendix*, Eq. **S12** for the relationship between D_{eff} and the experimental parameter, m). Note that, in the limit of small Δt and Δx, this discrete model is equivalent to the well-known equation proposed by Fisher, Kolmogorov, and Skellam to describe biological invasions:

$$\frac{\partial n}{\partial t} = D\frac{\partial^2 n}{\partial x^2} + nr(n). \quad [2]$$

Thus, our experiments can be viewed as both mimicking metapopulation dynamics typical for many ecosystems and approximating the continuous dynamics frequently assumed in mathematical ecology.

The dynamics of pulled expansions are completely determined by linearized growth $[g_{\Delta t}(n_{t,x}) \approx n_{t,x}e^{r_0\Delta t}; r_0 = r(n=0)]$ and the expansion velocity is given by

$$v_{lin} = \min_{\lambda>0}\left\{\frac{1}{\lambda\Delta t}\ln\left[e^{r_0\Delta t}\left[1 + \frac{D_{eff}\Delta t}{\Delta x^2}(\cosh(\lambda\Delta x) - 1)\right]\right]\right\} \approx 2\sqrt{r_0 D}, \quad [3]$$

where the population density at the front decays exponentially with a rate λ, such that the velocity is minimized (*SI Appendix*, Eq. **S10**). In the limit of vanishing Δt and Δx, this gives the classic Fisher velocity, $v = 2\sqrt{r_0 D_{eff}}$, and the spatial decay rate of the population density at the expansion edge, $\lambda = \sqrt{r_0/D_{eff}}$.

In sharp contrast, the knowledge of linearized growth is not sufficient to determine the velocity of a pushed expansion, because immigration from fast-growing regions behind the front increases the rate of invasion. Therefore, the deviations between the velocity and decay rate observed in the experiment and the corresponding values given by Eq. **3** indicate that the expansion is pushed, not pulled. In our analysis, we use this difference between the observed expansion velocity and the linearized growth velocity to distinguish between pulled and pushed waves.

Testing the Theory of Pulled Waves. A surprising prediction for pulled waves is that the emergent properties of the wave front, its velocity (v) and spatial decay rate (λ), depend on the per capita growth rate of the population only at low density, r_0, and not at higher densities. To the first order, $v \propto \sqrt{r_0}$, and consequently, an apparently healthy population that grows to a very high carrying capacity can in fact be a poor invader if it grows slowly, compared with a fast-growing population that saturates at lower densities. To test this hypothesis, we compared the range expansion of *S. cerevisae* in two different media: 0.125% glucose and 0.5% galactose. In both media, growth was exponential at low densities (Fig. 2*A*), but the two carbon sources showed a trade-off between faster low-density

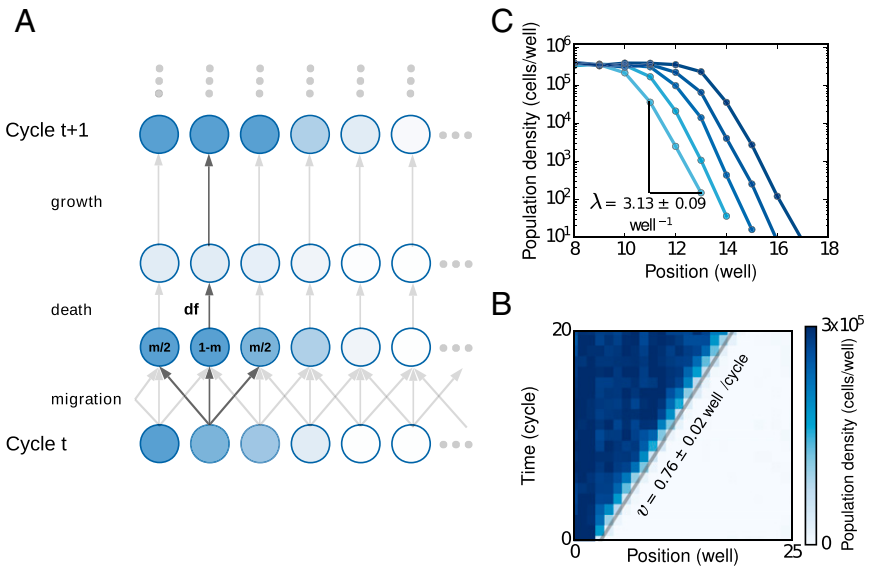

Fig. 1. Theoretical predictions for the velocity and spatial density profile of pulled and pushed waves were quantitatively tested in metapopulations of budding yeast, *S. cerevisae*, in a controlled experimental setup. (*A*) Yeast populations expanded along the columns of a 96-well plate. The experiments were started with an exponentially decaying spatial density profile. After every growth cycle of 4 h, cells were diluted into fresh media (dilution factor, df) and dispersal was achieved by transferring small amounts of media to neighboring wells along the columns. (*B*) Optical density measurements at the end of each cycle revealed an emergent wave traveling at constant velocity. (*C*) At later times, after allowing the fronts to equilibrate, the density profiles were also measured using flow cytometry. These high-resolution measurements at the low density fronts showed exponential fronts extending over four orders of magnitude in density. The spatial decay rate, λ, was estimated by averaging over density profiles over the last few cycles, after the expansion wave had equilibrated. The profiles measured using flow cytometry were also used to measure the velocity more accurately (*Materials and Methods*).

growth versus higher carrying capacity. Specifically, yeast cells initially grew at a faster rate in glucose but saturated to a lower carrying capacity compared with galactose (Fig. 2*B*). Furthermore, there was not a measurable Allee effect in either medium (*SI Appendix*, Fig. S2), and so we expected the expansions in both media to be pulled, and hence dependent only on the low-density growth rate. Consistent with the pulled-wave prediction, the resulting expansion waves indeed had a higher velocity in glucose, even though the bulk grew to a larger density in galactose (Fig. 2*C*).

To further quantify the qualitative agreement with theory that we observed above, we repeated the range-expansion experiment in a wide range of environmental conditions, with the same two media, 0.125% glucose or 0.5% galactose. We varied the migration rate ($m = 0.4, m = 0.5$) and the death rate (dilution factors of 2, 2.5, 3.3, and 4), which resulted in invasion velocities ranging from 0.2 wells per cycle up to 0.9 wells per cycle. Because the growth rate at very low densities needs to be known accurately, flow cytometry was used to count the number of divisions (fold growth) that cells undergo over the course of each 4-h cycle (*SI Appendix*, Figs. S2 and S10). We found excellent agreement between the experimentally observed velocities and the linearized growth velocities predicted based on the rates of dispersal and growth at low densities alone (Fig. 3*A*). Although this agreement is expected given the near-logistic growth in glucose and galactose, it provides a quantitative confirmation of the theory of pulled waves.

A similar comparison between the observed and predicted spatial decay rates was more challenging due to stochastic effects and long equilibration times. Stochastic effects appear due to the small number of individuals at the front and create much larger deviations between the deterministic theory (Eq. **1**) and the actual population dynamics for the spatial decay rate compared to the velocity (*SI Appendix*, Fig. S4). These deviations are known to make the fronts steeper (larger λ) (53, 54). Instead of using the analytical approximations that account for the stochastic effects, we chose a more direct and precise approach to test the theory of pulled waves. Because the distinction between pulled and pushed waves lies only in the degree to which the growth dynamics can be linearized, we performed individual-based simulations that included demographic fluctuations using only the growth rate measured at low densities. For pulled, but not pushed, waves the observed velocity and spatial decay rates must match simulations. As expected for expansions in glucose and galactose environments, the observed spatial decay rate was generally close to simulated values, confirming that these expansions are pulled (Fig. 3*B*). However, moderate deviations were observed under some experimental conditions. All four of these outliers occurred when the predicted spatial exponent was much smaller than that of the initial profile. As a result, these expansion profiles required a much longer time to reach their equilibrium shape and could still be out of equilibrium by the end of our experiments. Thus, the observed deviations might be due to insufficient observation time rather than the deviations from the theory of pulled waves.

Expansions Transition from Pulled to Pushed as Cooperativity Increases. Populations in which the per capita growth rate decreases monotonically with increasing density always expand as pulled waves (55); similarly, expansions of populations with a strong Allee effect are always pushed (17). However, populations with a weak Allee effect may be either pulled or pushed, depending on the magnitude of the Allee effect (Fig. 4*A*). Thus, the transition from pulled to pushed

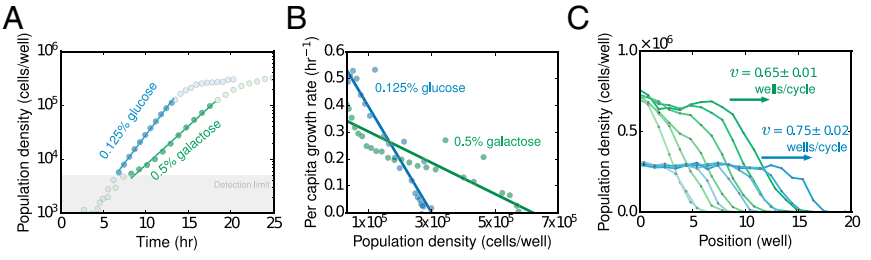

Fig. 2. In pulled waves, expansion velocity depends on the growth rate only at low densities irrespective of the carrying capacity. (*A*) A population of *S. cerevisae* grows exponentially at low densities in 0.125% glucose and 0.5% galactose. Growth rate at low densities is higher on 0.125% glucose compared with 0.5% galactose and decreases monotonically in both environments. (*B*) The galactose environment has a higher carrying capacity compared with glucose. The two environments thus show a trade-off between the low-density growth rate and the carrying capacity. (*C*) Although the galactose environment is more favorable in terms of the total nutrient availability (carrying capacity), expansions are faster in glucose because the populations grow faster in glucose at low density.

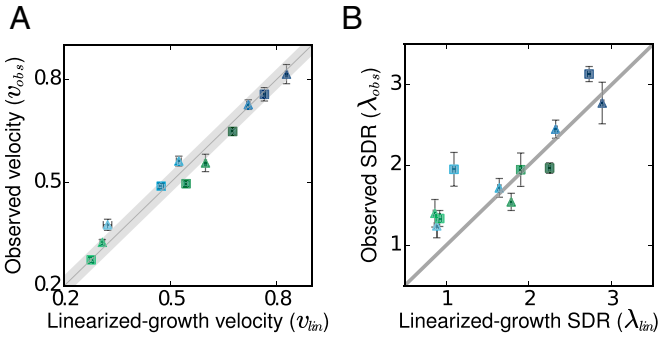

Fig. 3. For pulled waves, the growth rate at low density is sufficient to determine the emergent wave properties quantitatively. Over a wide range of environmental conditions, the observed expansion velocities and the spatial decay rates (SDR) of the population density at the front closely match the predictions based on the measured low-density growth rate. (*A*) Predicted and observed velocities in two different media are shown (glucose in blue, galactose in green). The migration rate (triangles: $m = 0.5$, squares: $m = 0.4$) and the death rate (darker colors are smaller death rates) were varied. Independently measured growth rates, only at low densities, in the two different media were sufficient to predict the velocities accurately. (*B*) A similar comparison for the spatial decay rates (λ, well^{-1}) also shows close agreement for steep predicted fronts (large λ). However, shallow predicted fronts deviated slightly from predictions, which may be a consequence of the long relaxation time to equilibrium for such fronts. *x*-axis error bars: SEM of the measured low-density growth rates, propagated to the errors in predicted velocity (*A*) and spatial decay rate (*B*). *y*-axis error bars: (*A*) SD of velocity measured for five different thresholds, and (*B*) SD in spatial decay rate measured over three different regions of the front.

waves occurs at some intermediate magnitude of the Allee effect, within the weak Allee effect regime (Fig. 4*B*).

To study this transition from pulled to pushed waves with increasing magnitude of the Allee effect, we studied the expansion of yeast when growing on the sugar sucrose, where growth is known to be cooperative. In our experiments, low-density growth rate measurements in 2% sucrose showed an Allee effect over densities ranging from ~10^3 to 10^5 cells per well, where the per capita growth rate increased with cell density (Fig. 5*A*). We note that this region of inverse density dependence is two orders of magnitude below the carrying capacity. As a result, the Allee effect would not have been visible with optical density measurements alone, and it was only revealed by fold-growth measurements using flow cytometry—a situation that parallels the difficulty of detecting Allee effects in natural populations. We show below that even this weak Allee effect was sufficient to make the expansion in 2% sucrose pushed instead of pulled.

We tuned the magnitude of the Allee effect by modulating the amount of sucrose in the media. As the sucrose concentration is increased, the growth rate at very low densities increases slowly, because only a fraction of the hydrolysis products can be captured by the cells before they diffuse away (*SI Appendix*, Fig. S5). In contrast, the maximal per capita growth rate, observed at intermediate cell densities, increases much more rapidly because dense populations use sucrose more efficiently (*SI Appendix*, Fig. S10). As a result, the magnitude of the Allee effect, measured as the difference between the low-density and the maximal per capita growth rate, increases with increasing sucrose concentration (*SI Appendix*, Fig. S6). Because the migration rates were known and the low-density growth rates were measured, we could directly compute the linearized growth velocity in each of the environments and compare it to the experimentally measured rate of invasion. For sucrose concentrations below ~0.025%, the observed velocities were close to the linearized growth velocities, indicating that the expansions were pulled. However, as the Allee effect increased in magnitude, the observed and linearized growth velocities started to differ, reflecting the transition to pushed expansions (Fig. 5*B*).

To confirm that the observed differences between the pushed and the pulled waves were statistically significant, we focused on expansions in glucose (pulled waves) and three sucrose concentrations: 0.22%, 0.67%, and 2% (pushed waves). Whereas the velocities of pulled waves fluctuated in a small region around the linearized growth velocities due to demographic and environmental stochasticity, the expansion velocities at high sucrose concentrations were much larger than, and well separated from, the corresponding linearized growth velocities ($P = 0.0015$; Fig. 5*C*). Thus, our experiments indeed demonstrated a transition from pulled to pushed waves.

A mechanistic model of yeast growth further confirmed that the departure from the theory of pulled waves resulted from an Allee effect due to the cooperative breakdown of sucrose (*SI Appendix*, section 3). Briefly, we assume that yeast cells consume glucose and grow following Monod kinetics. Small amounts of glucose are present initially, but the bulk of glucose is produced through sucrose hydrolysis with a rate proportional to the total yeast concentration. The collective hydrolysis gives rise to an increasing Allee effect with increasing sucrose concentration, and the model generically predicts a transition from pulled to pushed waves (*SI Appendix*, Fig. S7). We inferred the model parameters from the measurements of yeast growth rates across different cell densities and sucrose concentrations (*SI Appendix*, section 4). The model, thus parameterized, predicted expansion velocities that closely matched our experimental observations (Fig. 5*B*), demonstrating that the transition from pulled to pushed waves was indeed caused by a greater Allee effect at higher sucrose concentrations. Further supporting this conclusion, our estimates of the model parameters agreed well with previous measurements (*SI Appendix*, Table S1).

To demonstrate an important difference between pulled and pushed waves, we compared a pulled expansion in glucose to a pushed expansion in sucrose with the same velocity and dispersal rate. If both waves are pulled, the density profiles must have identical spatial decay rates, but if the expansion in sucrose is pushed, then it must have a steeper front. Keeping all other experimental parameters the same, the two media allowed such a

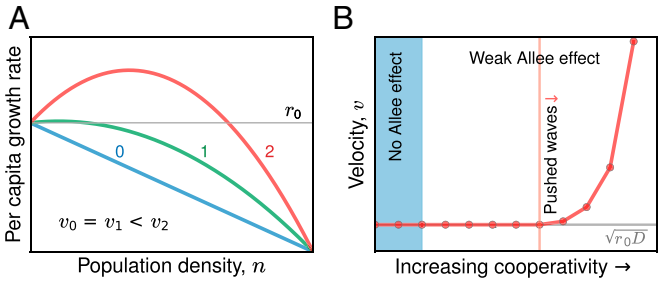

Fig. 4. Expansions transition from pulled to pushed waves at an intermediate strength of Allee effect within the weak regime. (*A*) Three different growth profiles displaying increasing magnitude of Allee effect (growth profile 0 is purely logistic; 1 and 2 have a weak Allee effect), but with the same low-density growth rate. Unlike pulled waves, the velocities of expansion in the three cases are not the same. In particular, both logistic (0) and the less-severe Allee effect (1) result in pulled waves with the same velocity, given by $2\sqrt{r_0 D}$. In contrast, condition 2, with a larger but still weak Allee effect, leads to a pushed wave with velocity greater than $2\sqrt{r_0 D}$. (*B*) In a generic model of the Allee effect (*SI Appendix*, Eq. **S13**), it can be shown that the transition from pulled to pushed waves occurs at a threshold magnitude of Allee effect that is different from the onset of a weak Allee effect. *B* shows the theoretical prediction for expansion velocity as the magnitude of the Allee effect (difference between maximal and low density per capita growth rate) is increased slowly, keeping the growth rate at low density constant. No change is seen in the dynamics of the expansion when a weak Allee effect is introduced. However, as the magnitude of the Allee effect is increased further, the expansion dynamics undergo a transition at a threshold magnitude of the Allee effect (vertical red line). The red curve is the actual expansion velocity, and the gray line is the velocity of a pulled wave with the same low density growth rate, r_0.

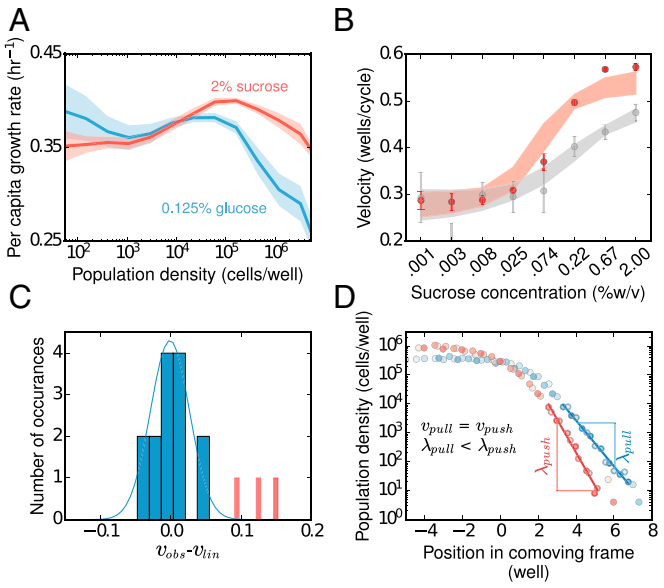

Fig. 5. Populations expand as pulled waves when Allee effect is small, but a large Allee effect makes populations expand faster than predicted based on linearized growth. (*A*) Experimental measurement of growth rates in sucrose (red) and glucose (blue). The growth rate in glucose decreases monotonically with increasing population density, and thus exhibits no Allee effect. In contrast, the per capita growth rate in sucrose increases with population density (between 10^3 and 10^5 cells per well) and thus exhibits a weak Allee effect. (*B*) By adding sucrose to the growth media, we increased the strength of the Allee effect (*SI Appendix*, Fig. S6) and observed a transition from pulled to pushed waves. Below sucrose concentration of 0.025%, observed expansion velocities (red dots) matched pulled-wave predictions based on linearized-growth (gray dots). For higher sucrose concentrations, we observed a significant deviation in observed velocities from the linearized growth velocities, indicating that expansions had become pushed. The error bars on the measured velocity (red points) are SD. Error bars are obtained on the linearized growth velocities (in gray) by bootstrapping on the growth rate measurements at low density. The observed velocities match well with the predictions of a mechanistic model (*SI Appendix*, section 4) shown in red shading. The model also captures the transition from pulled to pushed waves as the deviation between observed and linearized-growth velocities (gray shading) around sucrose concentration of 0.025%. The width of the shaded regions is the SD of simulation results for 89 parameter sets obtained by bootstrapping over the growth rate measurements and fitting the model to it. (*C*) The data at low sucrose concentrations (0.001, 0.003, and 0.008%; pulled regime) in blue and high sucrose concentrations (0.22, 0.67, and 2.0%; pushed regime) in red demonstrates the statistical significance of our results. When the Allee effect is small the difference in observed and linearized growth velocities is indistinguishable from zero, but the difference is large and highly significant for a large Allee effect (P = 0.0015). (*D*) Pushed waves are expected to have steeper profiles than pulled waves when expanding at the same velocity (and with the same migration rate). We found that a pulled wave in 0.125% glucose (blue) and a pushed wave in 2% sucrose (red) have approximately equal velocities, and, as expected, population densities declined much faster in space for the pushed wave.

comparison: 0.125% glucose and 2% sucrose. The low-density growth rate in 0.125% glucose was marginally higher than in 2% sucrose (Fig. 5*A*), and the velocity of expansion in both the glucose and sucrose environments was nearly the same within measurement error. However, the spatial decay rates of the wave fronts were very different for the two waves. As predicted, the wave profile in sucrose was steeper than that in glucose, providing additional support to our finding that expansion in sucrose was a pushed wave (Fig. 5*D*) and demonstrating that the differences in the decay rates can also be used for distinguishing pushed from pulled expansions.

Discussion

Although range expansions have been studied extensively in ecology, many theoretical predictions remain untested. Because pulled and pushed waves appear qualitatively similar, with a constant expansion velocity and exponential fronts, expansions are often assumed to obey the universal theory of pulled waves. Our study provides a proof of principle that pulled and pushed waves can be distinguished with quantitative measurements. We demonstrated that these two classes of expansions can be empirically distinguished based on the violation of the expected relationship between the velocity and either the front shape or the low-density growth rate. At the same time, our work also shows that such measurements are difficult even in controlled laboratory settings.

Distinguishing between pushed and pulled expansions is important for forecasting invasion dynamics and understanding species evolution. Predicting the rate of colonization may be particularly challenging for pushed waves because they can advance slowly in the beginning due to an Allee effect but accelerate later as the bulk density increases (47, 56). Pushed waves are also expected to have slower rates of neutral evolution and diversity loss compared with pulled expansions (26, 57). The conservation strategies to limit pulled and pushed invasions could also be very different. For pulled waves, the best way to limit the expansion is to eradicate the invaders at the very edge of the expansion. In contrast, a balanced eradication strategy over the entire invasion front is more effective for pushed waves (47, 58).

Beyond the specific results described above, our work established a tractable experimental system where many ecological and evolutionary scenarios or theories can be tested. Given the increasing rate of range shifts, it is important to experiment with how populations respond to unavoidable changes in their spatial distribution as well as to specific ecological perturbations designed as mitigation measures. Laboratory microbial systems could be very useful for studying such phenomena in greater detail, complementing more realistic but less tractable field studies.

Some questions that can be immediately investigated in our experimental system are the response of invasions to environmental fragmentation and the effects of range expansions on species evolution. Habitat fragmentation is likely to increase due to anthropogenic activities and might be especially important for species moving to barely hospitable regions as they escape the warming climate. Theory predicts that pushed, but not pulled, waves can become pinned or stuck in a fragmented environment, yet empirical tests of this prediction are scarce. Species evolution also depends critically on whether it invades as a pulled or a pushed wave. For example, the founder effect has a much greater role in pulled compared with pushed invasions. Quantitative experiments in controlled laboratory settings are likely to provide valuable insights into these important phenomena.

Materials and Methods

Strains. The yeast strain used is the same as the cooperator strain in ref. 59, derived from haploid cells BY4741 [mating type a, European Saccharomyces Cerevisiae Archive for Functional Analysis (EUROSCARF)]. It has a yellow fluorescent protein (yEYFP) expressed constitutively by the TEF1 promoter inserted into the HIS3 locus using the backbone plasmid pRS303.

Experimental Protocols. All cultures were grown at 30 °C in standard synthetic media (yeast nitrogen base and complete supplement mixture). The two media used for pulled wave experiments had 0.125% glucose and 0.5% galactose. The media used for studying the transition from pulled to pushed waves consisted of 0.008% background glucose (to reduce the sensitivity of the low-density growth rate to sucrose hydrolysis), in addition to 2, 0.67, 0.22, 0.07, 0.025, 0.008, 0.003, and 0.001% sucrose. All concentrations throughout the text are in percent weight per volume.

All experiments were performed in 200-μL batch culture in BD Biosciences Falcon 96-well Microtest plates. Range expansions were carried out along the columns of the plate, in 24- to 32-well-long landscapes. Migrations and dilutions were performed every 4 h using the Tecan Freedom EVO 100 robot. Plates were not shaken during growth. This resulted in a slightly lower growth rate and yield (58) compared with measurements in a platereader (compare Fig. 2 and *SI Appendix*, Fig. S2). Optical densities were measured on the robot before every dilution cycle in the Tecan Sunrise platereader

with 600-nm light. Cell densities for selected cycles were also measured in the MacsQuant flow cytometer after dilution in phosphate buffered saline (PBS), using the yellow fluorescence channel. Preliminary growth rate measurements on glucose and galactose were performed using overnight optical density measurements every 15 min. The more sensitive low-density growth rate measurements were performed in 96-well plates without shaking, by measuring initial and final cell densities over four dilution cycles of 4 h each, and ignoring the first two cycles for transient effects. Cultures were started at different initial densities for these measurements (*SI Appendix*, Fig. S10).

In the analysis, front positions were determined as the interpolated well position where the density (as measured by flow cytometry) crossed a fixed threshold. These were then used to calculate the velocity of expansion. The final velocity was obtained by averaging over multiple thresholds ranging between 100 and 1,000 cells per well. The thresholds were chosen so as to be sensitive to the dynamics at low density but at the same time not too low to be affected by Poisson errors in cell counting. Spatial decay rates were measured after translating the profiles at different times so that they coincide, and using the combined data to obtain a reliable fit to the exponentially decaying profile (Fig. 5*D*).

ACKNOWLEDGMENTS. We thank the members of the J.G. laboratory for helpful discussions and Jonathan Friedman and E.A.Y. for the flow cytometry data analysis tools. E.A.Y. was supported by a National Science Foundation (NSF) graduate fellowship. K.S.K. was supported by startup funding from Boston University. This work was funded by an Allen Distinguished Investigator Award, an NSF CAREER Award, and an NIH Director's New Innovator Award. J.G. has also received support as a Pew Scholar in the Biomedical Sciences and Sloan Fellow.

1. Hewitt G (2000) The genetic legacy of the Quaternary ice ages. *Nature* 405(6789): 907–913.
2. Graciá E, et al. (2013) The uncertainty of Late Pleistocene range expansions in the western Mediterranean: A case study of the colonization of south-eastern Spain by the spur-thighed tortoise, Testudo graeca. *J Biogeogr* 40(2):323–334.
3. Phillips BL, Brown GP, Greenlees M, Webb JK, Shine R (2007) Rapid expansion of the cane toad (Bufo marinus) invasion front in tropical Australia. *Austral Ecol* 32(2): 169–176.
4. Veit RR, Lewis MA (1996) Dispersal, population growth, and the Allee effect: Dynamics of the house finch invasion of eastern North America. *Am Nat* 148(2):255–274.
5. Levine JM, D'Antonio CM (2003) Forecasting biological invasions with increasing international trade. *Conserv Biol* 17(1):322–326.
6. Pateman RM, Hill JK, Roy DB, Fox R, Thomas CD (2012) Temperature-dependent alterations in host use drive rapid range expansion in a butterfly. *Science* 336(6084): 1028–1030.
7. Walther G-R, et al. (2002) Ecological responses to recent climate change. *Nature* 416(6879):389–395.
8. Pimentel D (2014) *Biological Invasions: Economic and Environmental Costs of Alien Plant, Animal, and Microbe Species* (CRC, Boca Raton, FL).
9. Mayo JH, Straka TJ, Leonard DS (2003) The cost of slowing the spread of the gypsy moth (Lepidoptera: Lymantriidae). *J Econ Entomol* 96(5):1448–1454.
10. Johnson DM, Liebhold AM, Tobin PC, Bjørnstad ON (2006) Allee effects and pulsed invasion by the gypsy moth. *Nature* 444(7117):361–363.
11. Sutherst RW, Floyd RB, Maywald GF (1996) The potential geographical distribution of the cane toad, Bufo marinus L. in Australia. *Conserv Biol* 10(1):294–299.
12. Leung B, Drake JM, Lodge DM (2004) Predicting invasions: Propagule pressure and the gravity of allee effects. *Ecology* 85(6):1651–1660.
13. Bocedi G, et al. (2014) RangeShifter: A platform for modelling spatial eco-evolutionary dynamics and species' responses to environmental changes. *Methods Ecol Evol* 5(4): 388–396.
14. Skellam JG (1951) Random dispersal in theoretical populations. *Biometrika* 38(1-2): 196–218.
15. Fisher RA (1937) The wave of advance of advantageous genes. *Ann Eugen* 7(4): 355–369.
16. Hanski I (1999) *Metapopulation Ecology* (Oxford Univ Press, Oxford).
17. van Saarloos W (2003) Front propagation into unstable states. *Phys Rep* 386(2–6): 29–222.
18. Murray JD, ed (1993) *Mathematical Biology* (Springer, New York).
19. Paquette GC, Chen L-Y, Goldenfeld N, Oono Y (1994) Structural stability and renormalization group for propagating fronts. *Phys Rev Lett* 72(1):76–79.
20. Courchamp F, Clutton-Brock T, Grenfell B (1999) Inverse density dependence and the Allee effect. *Trends Ecol Evol* 14(10):405–410.
21. Allee WC (1949) *Principles of Animal Ecology* (Saunders, Philadelphia).
22. Kramer AM, Dennis B, Liebhold AM, Drake JM (2009) The evidence for Allee effects. *Popul Ecol* 51(3):341–354.
23. Stephens PA, Sutherland WJ, Freckleton RP (1999) What is the Allee effect? *Oikos* 87(1):185–190.
24. Kot M (2001) *Elements of Mathematical Ecology* (Cambridge Univ Press, Cambridge, UK).
25. Hallatschek O, Nelson DR (2008) Gene surfing in expanding populations. *Theor Popul Biol* 73(1):158–170.
26. Korolev KS, Avlund M, Hallatschek O, Nelson DR (2010) Genetic demixing and evolution in linear stepping stone models. *Rev Mod Phys* 82(2):1691–1718.
27. Graciá E, et al. (2013) Surfing in tortoises? Empirical signs of genetic structuring owing to range expansion. *Biol Lett* 9(3):20121091.
28. Hundertmark KJ, Daele LJV (2009) Founder effect and bottleneck signatures in an introduced, insular population of elk. *Conserv Genet* 11(1):139–147.
29. Ramachandran S, et al. (2005) Support from the relationship of genetic and geographic distance in human populations for a serial founder effect originating in Africa. *Proc Natl Acad Sci USA* 102(44):15942–15947.
30. Lewis MA, Kareiva P (1993) Allee dynamics and the spread of invading organisms. *Theor Popul Biol* 43(2):141–158.
31. Melbourne BA, Hastings A (2009) Highly variable spread rates in replicated biological invasions: Fundamental limits to predictability. *Science* 325(5947):1536–1539.
32. Wakita J, Komatsu K, Nakahara A, Matsuyama T, Matsushita M (1994) Experimental investigation on the validity of population dynamics approach to bacterial colony formation. *J Phys Soc Jpn* 63(3):1205–1211.
33. Giometto A, Rinaldo A, Carrara F, Altermatt F (2014) Emerging predictable features of replicated biological invasion fronts. *Proc Natl Acad Sci USA* 111(1):297–301.
34. Jessup CM, et al. (2004) Big questions, small worlds: Microbial model systems in ecology. *Trends Ecol Evol* 19(4):189–197.
35. Momeni B, Brileya KA, Fields MW, Shou W (2013) Strong inter-population cooperation leads to partner intermixing in microbial communities. *eLife* 2:e00230.
36. Ben-Jacob E, et al. (1995) Complex bacterial patterns. *Nature* 373(6515):566–567.
37. Pirt SJ (1967) A kinetic study of the mode of growth of surface colonies of bacteria and fungi. *J Gen Microbiol* 47(2):181–197.
38. Korolev KS, et al. (2012) Selective sweeps in growing microbial colonies. *Phys Biol* 9(2): 026008.
39. Datta MS, Korolev KS, Cvijovic I, Dudley C, Gore J (2013) Range expansion promotes cooperation in an experimental microbial metapopulation. *Proc Natl Acad Sci USA* 110(18):7354–7359.
40. Korolev KS (2013) The fate of cooperation during range expansions. *PLOS Comput Biol* 9(3):e1002994.
41. Chen L, et al. (2014) Two-dimensionality of yeast colony expansion accompanied by pattern formation. *PLOS Comput Biol* 10(12):e1003979.
42. Van Dyken JD, Müller MJI, Mack KML, Desai MM (2013) Spatial population expansion promotes the evolution of cooperation in an experimental Prisoner's Dilemma. *Curr Biol* 23(10):919–923.
43. Weber MF, Poxleitner G, Hebisch E, Frey E, Opitz M (2014) Chemical warfare and survival strategies in bacterial range expansions. *J R Soc Interface* 11(96):20140172.
44. Kerr B, Riley MA, Feldman MW, Bohannan BJM (2002) Local dispersal promotes biodiversity in a real-life game of rock-paper-scissors. *Nature* 418(6894):171–174.
45. Hallatschek O, Hersen P, Ramanathan S, Nelson DR (2007) Genetic drift at expanding frontiers promotes gene segregation. *Proc Natl Acad Sci USA* 104(50):19926–19930.
46. Korolev KS, Xavier JB, Nelson DR, Foster KR (2011) A quantitative test of population genetics using spatiogenetic patterns in bacterial colonies. *Am Nat* 178(4):538–552.
47. Taylor CM, Hastings A (2005) Allee effects in biological invasions. *Ecol Lett* 8(8): 895–908.
48. Keitt TH, Lewis MA, Holt RD (2001) Allee effects, invasion pinning, and species' borders. *Am Nat* 157(2):203–216.
49. Gore J, Youk H, van Oudenaarden A (2009) Snowdrift game dynamics and facultative cheating in yeast. *Nature* 459(7244):253–256.
50. Dai L, Vorselen D, Korolev KS, Gore J (2012) Generic indicators for loss of resilience before a tipping point leading to population collapse. *Science* 336(6085):1175–1177.
51. Sanchez A, Gore J (2013) Feedback between population and evolutionary dynamics determines the fate of social microbial populations. *PLoS Biol* 11(4):e1001547.
52. Koschwanez JH, Foster KR, Murray AW (2011) Sucrose utilization in budding yeast as a model for the origin of undifferentiated multicellularity. *PLoS Biol* 9(8):e1001122.
53. Brunet É, Derrida B (2001) Effect of microscopic noise on front propagation. *J Stat Phys* 103(1–2):269–282.
54. Brunet E, Derrida B (1997) Shift in the velocity of a front due to a cutoff. *Phys Rev E Stat Phys Plasmas Fluids Relat Interdiscip Topics* 56(3):2597–2604.
55. Kolmogorov AN, Piscounov N, Petrowski I (1937) Étude de l'équation de la diffusion avec croissance de la quantité de matière et son application a un problème biologique. *Mosc Univ Bull Math* 1:1–25.
56. Liebhold AM, Tobin PC (2006) Growth of newly established alien populations: Comparison of North American gypsy moth colonies with invasion theory. *Popul Ecol* 48(4):253–262.
57. Roques L, Garnier J, Hamel F, Klein EK (2012) Allee effect promotes diversity in traveling waves of colonization. *Proc Natl Acad Sci USA* 109(23):8828–8833.
58. Tobin PC, Berec L, Liebhold AM (2011) Exploiting Allee effects for managing biological invasions. *Ecol Lett* 14(6):615–624.
59. Celiker H, Gore J (2012) Competition between species can stabilize public-goods cooperation within a species. *Mol Syst Biol* 8:621.

Range expansions transition from pulled to pushed waves as growth becomes more cooperative in an experimental microbial population

Saurabh R. Gandhi[1], Eugene Yurtsev[1], Kirill S. Korolev[2*], Jeff Gore[1*]

[1] Physics of Living Systems Group, Department of Physics, Massachusetts Institute of Technology, Cambridge, MA 02139, USA

[2] Department of Physics and Graduate Program in Bioinformatics, Boston University, Boston MA, 02215, USA

[*]Corresponding authors: [2]korolev@bu.edu, [1]gore@mit.edu

Supplementary Information Appendix

1. Reaction-diffusion models for one-dimensional range expansions

Populations expanding via short-range migration in one spatial dimension are often modeled by a reaction-diffusion equation, which is continuous in space and time:

$$\frac{\partial n}{\partial t} = D\frac{\partial^2 n}{\partial x^2} + nr(n). \qquad \text{S1}$$

Here $n(x,t)$ is the density of population at position x at time t; D is the dispersal coefficient, which is assumed to be constant in the simple model, and $r(n)$ is the density-dependent per capita growth rate of the population. Many properties of this model can be obtained analytically by linearizing the growth term, $nr(n) \approx nr(0)$ at low densities (Fig. S1); we will also denote $r(0)$ as r_0. When colonization dynamics are determined by the dynamics at the expansion edge, this approximation is quite accurate because population densities are low at the expansion front. Kolmogorov *et. al.* proved that, when $r(n)$ is a monotonically decreasing function, this linearization is guaranteed to capture the expansion dynamics (55). Expansions described by the linearized growth term are called pulled because they advance via growth at the low-density front, which effectively pulls the waves forward. Importantly, the condition derived by Kolmogorov *et. al.* is sufficient but not necessary. In particular, the linear approximation continues to hold even when a small Allee effect is present. For larger Allee effects, dispersal from the faster growing high density region of the front dominates the growth at the low-density expansion edge,

effectively pushing the wave forward. These 'pushed' waves advance at a higher velocity than one would predict using just $r(0)$ (17).

Although the model (eqn. S1) can be analyzed in numerous ways (17, 18, 24), a solution using Fourier transforms is most useful for extending the results to the case of discrete space and time systems, such as in our experiments. Here, we briefly outline the solution to the continuous model using Fourier modes as described by van Saarloos (17). We then apply a similar analysis to a model appropriate for our experimental system, which was used to predict the linearized-growth-velocities in the main text.

The spatial Fourier modes of the front can be written as:

$$\tilde{n}(q,t) = \int_{-\infty}^{\infty} dx n(x,t) e^{-iqx} \quad \text{S2}$$

where q is the wave number of the Fourier modes. To obtain the spreading speed of a front, we start with an Ansatz assuming the Fourier modes are of the form $\tilde{n}(q,t) = \tilde{n}(q)e^{-i\omega(q)t}$. Substituting back in eqn. S1 gives the dispersal relationship ($\omega(q) = i(r_0 - Dq^2)$). Assuming that the front moves with some constant asymptotic velocity, v^*, we perform inverse Fourier transforms in the coordinate frame moving with the front ($\zeta = x - v^*t$):

$$n(\zeta,t) = \frac{1}{2\pi}\int_{-\infty}^{\infty} dq\, e^{iq\zeta - i[\omega(q) - v^*q]t} \quad \text{S3}$$

In the large time limit, only those modes near the saddle point of $[\omega(q) - v^*q]$ survive (60), which results in the following condition:

$$v^* = \left.\frac{d\omega}{dq}\right|_{q^*} \quad \text{S4}$$

where q^* is the saddle point. Further, in the co-moving reference frame, the wave profile neither grows nor decays in time, so the imaginary part of the exponent must vanish:

$$Im\big(\omega(q^*)\big) - Im(q^*)v^* = 0 \quad \text{S5}$$

This gives the set of relationships that can be used to calculate the asymptotic velocity:

$$v^* = \left.\frac{Im(\omega(q))}{Im\,(q)}\right|_{q^*} = \left.\frac{d\omega}{dq}\right|_{q^*} \quad \text{S6}$$

The above two relationships uniquely determine the asymptotic speed v and q^*. The exponential decay rate of the population density at the front then follows eqn. S3 since $\lambda = Im\,(q^*)$. The results are

$$v^* = 2\sqrt{r_0 D},\ \lambda = \sqrt{\frac{r_0}{D}}\ . \tag{S7}$$

2. Expansions in discrete space and time models

The discretized form (corresponding to the experimental protocol) of the F-KPP equation can be written as:

$$n_{x,t+\Delta t} = g_{\Delta t}\left(n_{x,t} + \frac{m}{2}\left(n_{x+\Delta x,t} + n_{x-\Delta x,t} - 2n_{x,t}\right)\right), \tag{S8}$$

where x is the spatial coordinate, t is the cycle number, and $g_{\Delta t}(n)$ describes total growth rate, i.e. $g_{\Delta t}(n)$ is the product of the per capita growth rate and the population density. Upon linearization $g_{\Delta t}(n)$ can be written as:

$$g_{\Delta t}(n) = n\frac{e^{r_0 \Delta t}}{dilution}, \tag{S9}$$

which corresponds to exponential growth at rate r_0 followed by a dilution. Substituting the Fourier mode $\widetilde{n_x} = e^{iqx-i}$ in the above linearized equation gives the dispersion relation:

$$e^{-i\omega\Delta t} = \frac{e^{r_0 \Delta t}}{dilution}[1 + m(cosh(-iqx) - 1)] \tag{S10}$$

Following the analysis of the continuous case, we use the saddle point approximation and require that the front is not changing in the co-moving reference frame. The resulting equations are similar to eqn. S6 and can be recast in a simpler form with the definitions of two real parameters $\lambda = Im(q)$ and $s = Im(\omega)$ and an observation that these equations correspond to the requirement that

$$v = min_{\lambda>0}\left\{\frac{S}{\lambda}\right\};$$

compare to eqn. 3 in the main text.

For small Δt, one can analytically obtain corrections to the continuous results in eqn. S7 due to the discreteness of space. However, since in our experiments, $\Delta t \sim 4$ hrs, which is longer than the time scale

set by the growth rate (~2 hrs), the velocity and spatial decay rate have to be evaluated by minimizing eqn. S10 numerically.

The magnitude of deviations between the continuous and discrete models are shown in Fig. S3. Note that the discrete dynamical equation describing the experiment is not the same as the discretized version of the F-KPP equation, which can be written as:

$$n_{x,t+\Delta t} = n_{x,t} e^{r_{0,eff}\Delta t} + D_{eff}\frac{\Delta t}{\Delta x^2}\left(n_{x+\Delta x,t} + n_{x-\Delta x,t} - 2n_{x,t}\right) \quad \text{S11}$$

Comparing eqns. S9 and S11, the effective growth and diffusion rates in the continuous model should be expressed in terms of experimental parameters as follows:

$$r_{0,eff} = r_0 - \frac{ln(dilution)}{\Delta t}$$

$$D_{eff} = \frac{m}{2}\frac{\Delta x^2}{\Delta t}(1 + r_{eff}\Delta t) \quad \text{S12}$$

($\Delta t = 4$ hr, $\Delta x = 1$ well). The effective parameters can then be used in continuous models to compare them to the discrete space-time experimental model and evaluate the magnitude of 'corrections' that are introduced due to the discretization.

The finite number of organisms per spatial patch also changes the velocity and spatial decay rate. Although stochastic effects obviously cause fluctuations in the velocity, the expectation value of the velocity is also reduced as compared to predictions that do not incorporate demographic stochasticity. The deviations have been shown to be of the order of $\frac{1}{\log^2 N}$, where N is the number of individuals per unit length, when space and time are continuous (54). Moreover, the fronts have been shown to be steeper when demographic stochasticity is added (53, 54). We see this in our experiments, where, without accounting for the demographic stochasticity, the observed spatial decay rate is larger than predicted. This discrepancy vanished when we incorporated the effects of stochasticity in our predictions (Fig. S4).

3. Cubic model of the Allee effect

A generic model of the Allee effect was used for making the cartoon in Fig. 4 in the main text. In this model, the density dependence of growth is given by:

$$\frac{1}{n}\frac{dn}{dt} = \frac{r_0}{a}\left(1 - \frac{n}{k}\right)(n + a) \quad \text{S13}$$

This model shows no Allee effect for $a > k$ (per capita growth rate monotonically decreases with increasing density), and a weak Allee effect for $a < k$. Further, as a is varied, the growth rate at low density remains constant and is given by r_0. The transition from pulled to pushed waves occurs at $a = k/2$ inside the weak Allee effect regime (64).

4. A mechanistic growth model captures the Allee effect and shows a transition from pulled to pushed waves with increasing sucrose

We developed a mechanistic model for yeast growth in our experiments. The model incorporates previously well-studied mechanisms such as Monod growth on glucose (61) and a Michaelis-Menten kinetics of sucrose hydrolysis (49, 52, 63). Using previously measured values of the model parameters (Table S1), we found that the magnitude of the Allee effect increases with the amount of sucrose in the medium. Importantly, the model also displayed a transition from pulled to pushed waves, consistent with the experimental observations in Fig. 5 (Fig. S7). This transition was observed for a wide range of model parameters and is a generic prediction of the model. To test for quantitative agreement between the model and the experiments, we fitted the parameters of the model to our independent measurements of the growth rates, and confirmed that the predicted velocities closely match experimental observations (Fig. S8).

The model describes growth of yeast in the presence of glucose and sucrose, and assumes that there are no other limiting resources. Furthermore, while glucose is metabolized directly by the yeast, sucrose needs to be hydrolyzed to monosaccharides before it can be utilized. Although sucrose is hydrolyzed to glucose and fructose, we treat these sugars equivalently and refer to the combined concentration of the monosaccharides as the glucose concentration (49). This hydrolysis reaction is catalyzed by an enzyme invertase produced by yeast cells. Most of the invertase stays attached to the cell surface resulting in higher rates of hydrolysis in the immediate vicinity of the cell and creating a local cloud of glucose in

excess of the bulk glucose concentration. Thus, yeast cell benefit from both the glucose produced by themselves and from the glucose produced by their neighbors (49). These dynamics are captured by the following Monod growth law and glucose consumption equation:

$$\frac{1}{n}\frac{dn}{dt} = \frac{g_{loc}}{g_{loc}+k_g}\gamma_{max} \quad \text{S14}$$

$$\frac{dg}{dt} = -Y\frac{dn}{dt} + nV \quad \text{S15}$$

Here, the first equation describes cell division, where n is the cell density, g_{loc} is the local glucose concentration around each cell, k_g is the Michaelis-Menten constant for glucose utilization and γ_{max} is the maximum division rate. The second equation gives the corresponding rate of utilization of glucose (g), which is proportional to the division rate of the cells (the proportionality constant, Y, determines the carrying capacity of the population). The additional term, nV, corresponds to the production of glucose due to sucrose hydrolysis. The per capita rate of sucrose hydrolysis, V, is given by

$$V = v_s\frac{s}{s+k_s} = -\frac{1}{n}\frac{ds}{dt}, \quad \text{S16}$$

where s is the sucrose concentration, v_s is the maximum rate of sucrose hydrolysis, and k_s is the Michaelis-Menten constant. Finally, the local glucose concentration around the cell is the sum of the bulk glucose concentration, and the additional cloud of glucose due to the sucrose hydrolysis on the cell surface. The contribution of this cloud is proportional to the rate of sucrose hydrolysis, and thus

$$g_{loc} = g + g_{eff}V, \quad \text{S17}$$

where g_{eff} is the proportionality constant that accounts for the glucose escape through diffusion (49).

To infer model parameters, we measured growth rates in varying sucrose concentrations, and different cell densities. The growth rate measurements and the corresponding range expansions were carried out in 9 different media: 0.125% glucose, and 0.008% glu + varying amounts of sucrose.

Before we describe the specifics of how the model parameters were determined from the experimental data, it is important to discuss how each parameter contributes to the different aspects of the experimental data and demonstrate that the data contains sufficient information to constrain the model

parameters. The yield parameter, Y, determines the number of cells that can be produced given a certain amount of glucose. For the growth rate measurements in pure glucose, Y therefore controls the population densities at which the growth rate precipitously drops to zero. We determined Y by fitting the model prediction to our growth measurement at high cell densities in 0.125% glucose (Fig. S9). The growth rate at low cell densities in pure glucose media is completely determined by $\gamma_{max}\ and\ k_g$, and our data contained sufficient information to infer these parameters because we had low-density growth rate measurements in pure glucose as well as in several sucrose concentrations that produced varying local concentrations of glucose as specified by eqn. S17. The low-density growth rates at different sucrose concentrations also depend on $k_s\ and\ v_s g_{eff}$; therefore, we could use our low-density measurements to infer four model parameters $\gamma_{max}, k_g, k_s\ and\ v_s g_{eff}$.

The dynamics at high population densities depend not only on the product of v_s and g_{eff}, but on the individual values of these parameters. In particular, higher values of v_s and lower values of g_{eff} (keeping their product fixed) result in a larger Allee effect and more cooperative growth because of the faster sucrose hydrolysis and greater sharing of glucose via diffusion away from the cell. Therefore the magnitude of the Allee effect at high sucrose concentration provided the last necessary constraint to determine all of the model parameters.

Instead of directly fitting to the entire data set simultaneously, we used a modular approach of fitting the growth dynamics at low-density and high-density separately. We also bootstrapped on our data to determine the uncertainty in model parameters and model predictions.

To obtain a set of low density growth parameters, we bootstrapped over the measured values of growth rates in each of the media, and fitted the parameters by minimizing the squared distance from the bootstrapped data using Python package scipy (curve_fit). All data at starting densities below OD 0.004 was included, as indicated in Fig. S10. However, all outliers more than 2.5 SD away from the mean, were excluded from the analysis. Moreover, growth was unusually slow in one of the measurements, in 0.003%

sucrose. This is the regime where the low-density growth rate is independent of sucrose concentration, since the concentration of sucrose is lower than that of glucose, which was 0.008%. Therefore, we excluded this particular condition while fitting the parameters. The bootstrapping procedure was repeated to obtain 100 sets of low-density growth parameters, $\gamma_{max}, k_g, k_s \; and \; v_s g_{eff}$. Out of these, a few iterations of the curve_fit routine did not converge on the fit, leaving 89 sets of parameters for downstream analysis. Fig. S11 shows the low-density growth rates that the model predicts for each of the parameter sets.

Next, for each of the 89 sets obtained above, we determined the individual parameters, v_s and g_{eff}, keeping the product constant. As noted earlier, the relative magnitudes of these two parameters control the magnitude of the Allee effect. Therefore, parameters v_s and g_{eff} were determined by minimizing the squared distance from growth rates at intermediate densities in 2%, 0.67% and 0.22% sucrose – the media that exhibit a substantial Allee effect. The sum of squared distance from all the data points in the selected regions of the cell densities was calculated for values of v_s ranging from 0.2 to 4 % $OD^{-1}hr^{-1}$, and the value of v_s minimizing the sum was chosen. These regions of cell densities were selected such that the growth rates increase with density (i.e. exhibit an Allee effect) and are summarized below:

2% sucrose: OD $5x10^{-3}$ to $2x10^{-1}$,

0.67% sucrose: OD $5x10^{-3}$ to $2x10^{1}$,

0.22% sucrose: OD $5x10^{-3}$ to $3x10^{-1}$.

Table S1 shows a comparison between the previously reported values of the parameters for yeast, and the median parameter values that we have obtained by the procedure described above. The distribution of parameter values is shown in Fig. S12. Most of the fitted values were consistent with literature. The exception is g_{eff}, which is an order of magnitude larger than previously reported. However, this parameter depends strongly on the diffusion rate of glucose, such that slower diffusion leads to larger g_{eff}. Since the cells in our experiments are not being shaken (both during range

expansions as well as in the experiments we performed to measure growth rates), most of the hydrolysis products remain in the vicinity of the cell, resulting in lower diffusion, and a larger g_{eff}. Other factors that affect g_{eff} such as genetic background, cell size, etc. could also contribute to the observed difference with previous measurements. The lack of mixing is also consistent with the slightly lower v_s that we estimate compared to literature, since the efficiency of hydrolysis is reduced.

These 89 parameter sets fit the observed growth rates well over the entire range of cell densities and sucrose concentrations as shown in Fig. S13.

We then simulated expansions using the mechanistic growth model and the 89 parameter sets obtained above. The simulations exactly follow the experiments, and have cycles of migration/dilution followed by growth, with eqn. S14-S17 giving the dynamics in the growth phase (Fig. S14, SI section 5, SI simulation code). The simulated velocities for each of the 89 parameter sets all show a transition from pulled to pushed waves with increasing sucrose concentration, and are distributed closely around experimentally observed velocities (Fig. S8).

The excellent agreement between the model and the experimental observations further supports our conclusions that the break-down of the theory of pulled waves at high sucrose concentrations is due to an increasing strength of the Allee effect makes yeast expand as a pushed wave.

5. Simulations

Stochastic simulations were performed for computing the rate of exponential density decay at the front as well as for testing the predictions of the mechanistic growth model. In the simulations, the expansions were allowed to proceed for longer times than in the experiment, so as to completely remove all transients. Expansions were typically simulated for 60 cycles across a sufficiently long landscape so that the waves do not reach its edge. The total carrying capacity in each spatial patch was the same as in the experiments.

The simulations reflect exactly the dynamics in our experiments (Fig. S14). The cells start with an exponential spatial density profile. For each cycle, logistic model (in simulations for calculating the exponent at the front) or the mechanistic growth model is integrated over a period of 4 hours to obtain the final population density in each well. Growth is thus deterministic in the simulations. At the end of the growth cycle, the number of cells is rounded off to the nearest integer. Binomial sampling is used to determine the number of cells that are transferred for the next cycle, taking into account the migration rate as well as the dilution rate. This step therefore accounts for the demographic fluctuations.

Finally, since growth in the mechanistic model explicitly depends on sugar concentrations, we also include the effects of sugar transfer due to migration and dilution in the simulations (Fig. S14).

Velocities in the simulations are calculated in the same way as experiments (Materials and Methods). A threshold density of 2000 cells per well and the location of the wavefront is defined as the position at which the profile crosses this threshold. Velocity is then calculated by obtaining a linear fit between the position and time.

Parameter	**Median**	**Literature**	**References**
Maximal growth rate on glucose, γ_{max} [hr^{-1}]	0.390	0.3 – 0.55 (0.39)	39, 49-51
K_M for growth on glucose, k_g [% w/v]	0.0019	0.002 – 0.003 (0.002)	63
K_M for sucrose hydrolysis, k_s [% w/v]	0.781	0.5 – 1.5 (0.8)	49, 61-62
Maximal sucrose hydrolysis rate, v_s [% OD^{-1} hr^{-1}]	0.833	2.4 (2.4)	49
Privatization parameter, g_{eff} [OD hr]	0.02	0.0015 (0.0015)	49
Yield on glucose, Y [% OD^{-1}]	0.057	– (0.07)	–

Table S1

The table shows a comparison between previously reported and median values of model parameters obtained by fitting the model to measured growth rates. Values in brackets under the literature column are used for the simulation in Figure S7.

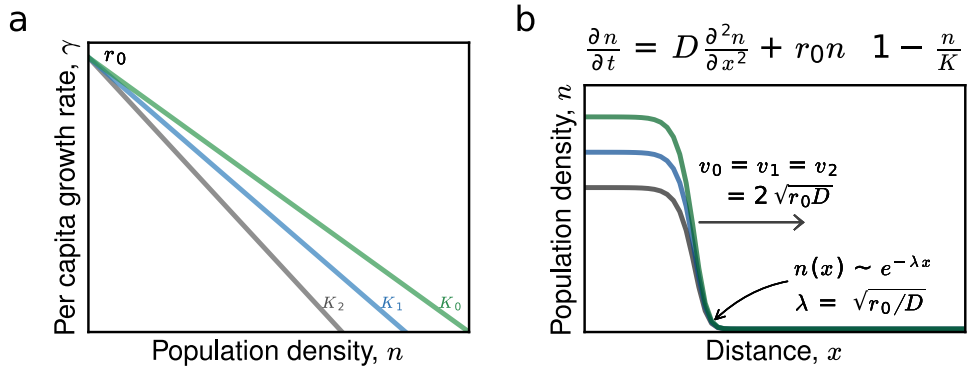

Figure S1
Reaction-diffusion equations are classical models for expansion in theoretical ecology. When populations grow logistically, Fisher's equation predicts traveling waves of constant velocity, with an exponential spatial profile near the front. Both of these emergent properties depend only on the low-density growth rate, and are independent of the carrying capacity.
(a) Populations that obey logistic growth increase exponentially with rate r_0 at low density, and the per capita growth rate decreases monotonically until the population density saturates at some carrying capacity, K. Three growth curves with identical low-growth rate, but different carrying capacities are shown. (b) Emergent properties of the expansion front, such as velocity (v) and spatial decay rate of density at the front (λ), depend only on the per capita growth rate at low density (r_0) and the diffusion constant (D), and are independent of the carrying capacity (v_0=v_1=v_2, λ_0=λ_1=λ_2=λ). The bulk density, however, does depend on the carrying capacity (K).

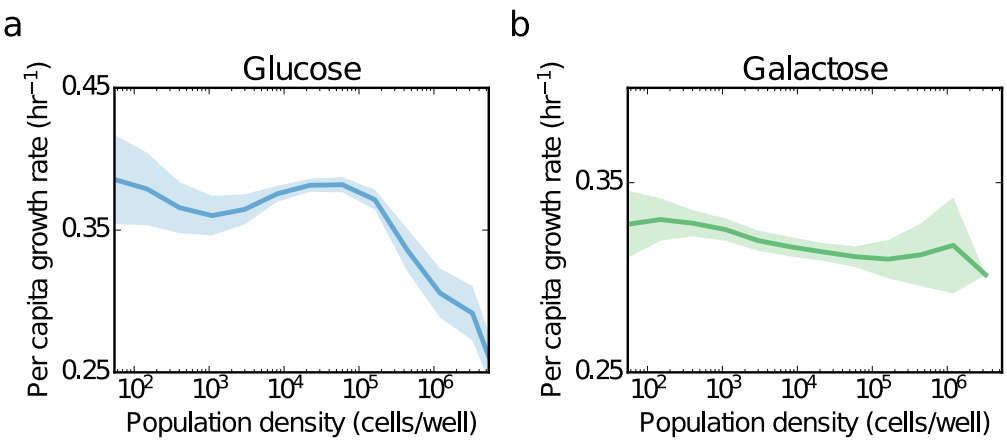

Figure S2
The maximal per capita growth rate in galactose (a) and glucose (b) never significantly exceeds the per capita growth rate at low density
We measured the fold growth by counting the number of yeast cells before and after 4 hours of growth in a 96-well plate. Each well started with a small number of yeast cells. After propagating the cultures with dilution for two 4-hour cycles (to remove transient effects caused by a change of growth environment), the number of cells in the wells were counted by flow cytometry at the beginning and end of the third and fourth cycle. Cells were counted after a 100x dilution. Due to the small numbers, the actual counts at low density had a large sampling noise. The figure shows the growth rate as an average over a Gaussian moving window. Shaded region indicates standard deviation in the average over the window in bootstrapped data. Since density does not change appreciably over the course of four hours, we estimated the growth rate assuming that it remains constant over the course of the experiment and results in an exponential increase in cell density.

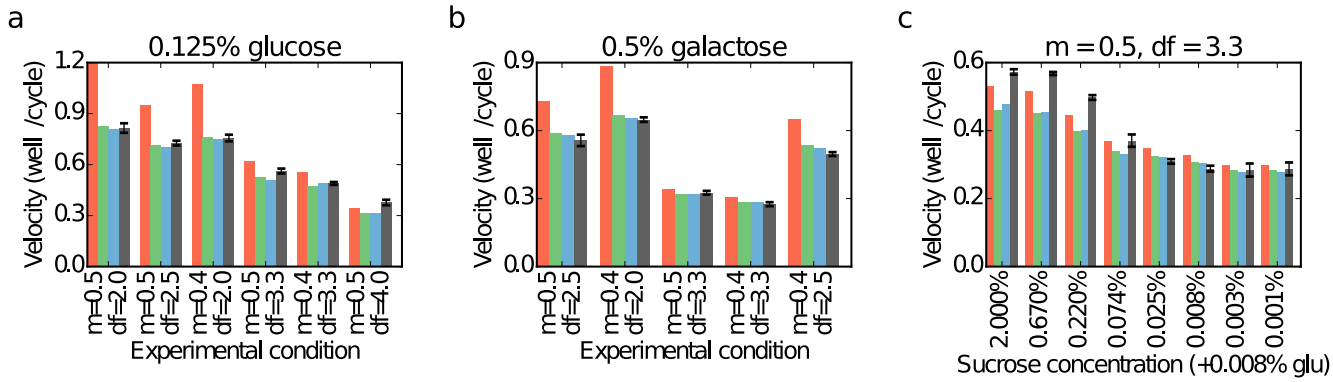

Figure S3
Effect of discretizing space and time (and addition of demographic stochasticity) on predicted velocities in glucose (a), galactose (b) and sucrose (c) environments. Each set of bars represents an experimental condition (different migration and death rates). In (c), the 8 conditions have constant migration and death rate, but decreasing amount of sucrose. Red bars indicate predicted linearized-growth-velocities in continuous space-time models with the same effective growth and diffusion rate as the discrete experimental system (eqn. S12). Here, we show a decomposition of the effects due to discrete space-time, and demographic stochasticity. Discreteness of space and time (green): Since migration is limited to one well at a time in the linear stepping stone model, emergent wave velocities can never exceed 1 well/cycle. The corrections are large and are calculated numerically from eqn. S10.
Demographic stochasticity (blue): Demographic stochasticity has been predicted to reduce expansion velocity. The correction to the continuous space-time model due to demographic stochasticity is of the order of $1/log^2(N)$. In our experiments, we calculated the corrections using simulations with measured growth rates and other known experimental parameters.
Experimental data (gray): We see that the observed velocities are in close agreement with predictions once the effects of discretization and stochasticity are incorporated (subplots a, b). Panel (c) shows that the observed and predicted velocities match for low but not high sucrose concentrations (even after incorporating the effects described above). The deviations are due to the large Allee effect at high sucrose concentrations, making the waves pushed. Error bars indicate S.D. in measured velocity at five different threshold densities.

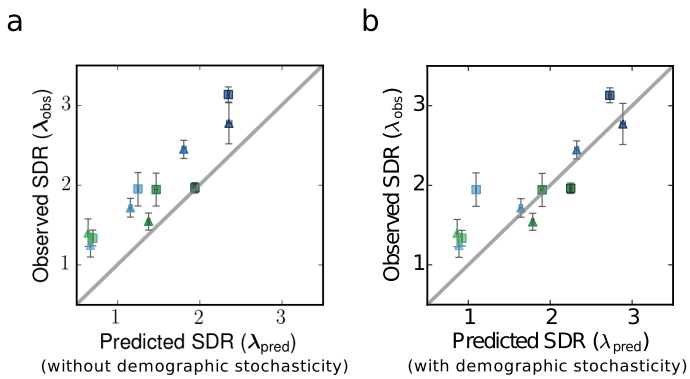

Figure S4
Demographic stochasticity significantly affects the spatial decay rate at the front (SI Section 2)
(a) Predicted spatial rate of decay at the front, based on linearized growth, is less than what is experimentally observed when demographic stochasticity is not taken into account. (b) When finite population effects (demographic stochasticity) are included, the observed front shape is close to predictions. The predicted spatial decay rate is based on simulations using measured values of low-density growth rate and known experimental parameters such as migration and death rate (SI section 5). y-axis error bars indicate S.D. in measured decay rate for three different fitting regions at the front.

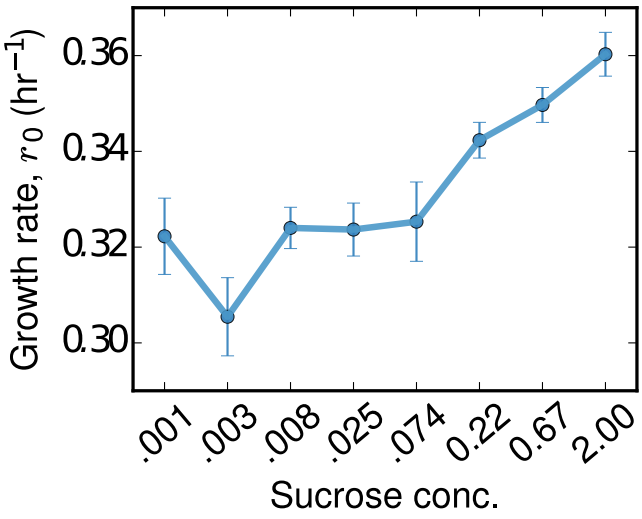

Figure S5
Low-density growth rate increases slowly with increasing sucrose concentration
Since some of the hydrolyzed sucrose is captured by the yeast cells before it can diffuse away, increasing the sucrose concentration leads to increased growth rates even at low densities, when cooperative effects are absent (SI section 4). However, the maximal growth rate increases faster than the low-density growth rate, resulting in an increasingly severe Allee effect (Fig. S6). Error bars indicate S.E.M. in measured low-density growth rates (Fig. S10).

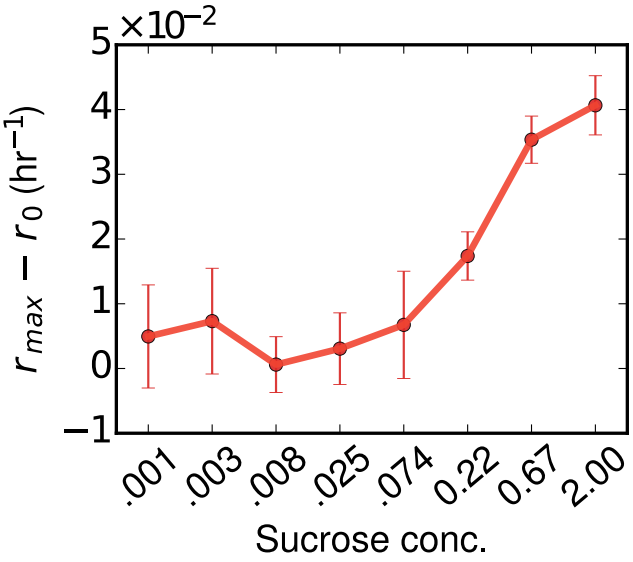

Figure S6
Magnitude of Allee effect increases with increasing sucrose concentration
The magnitude of the Allee effect is estimated as the difference between the maximal growth rate, r_{max}, and the low-density growth rate, r_0. Error bars indicate S.E.M. of the low-density growth rate (Δr_0). r_{max} was determined as the maximal value of the growth rate after averaging over a moving Gaussian window, as shown in Fig. S2 for 0.125% glucose and 0.5% galactose.

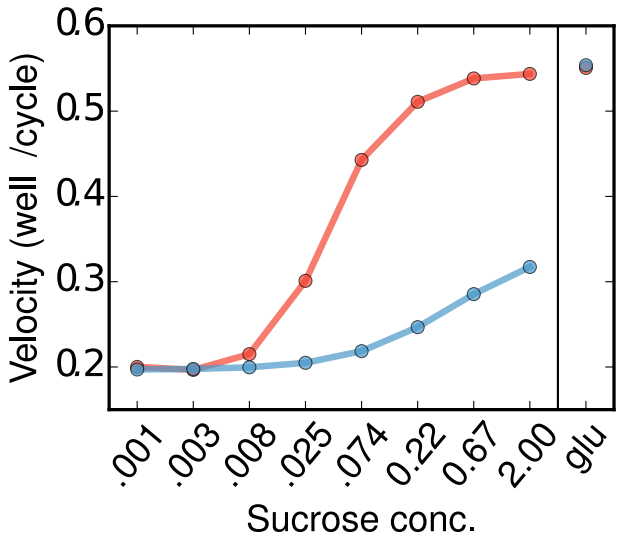

Figure S7
A mechanistic model of yeast growth on sucrose and glucose predicts a transition from pulled to pushed waves (SI section 4)
A simple mechanistic model where yeast grows on glucose following Monod kinetics, and hydrolyzes sucrose to glucose (details in SI) was used to simulate expansions. All the parameters in the model have been reported previously in various studies. Using typical parameter values from published literature (table S1), the model predicts a transition from pulled to pushed waves as the sucrose concentration in the media is increased. At low sucrose concentrations, expansions are pulled, reflected in the agreement between simulated velocities and the linearized-growth predictions. At larger sucrose concentrations, expansion velocities exceed the linearized-growth prediction, indicating that the expansions are pushed.

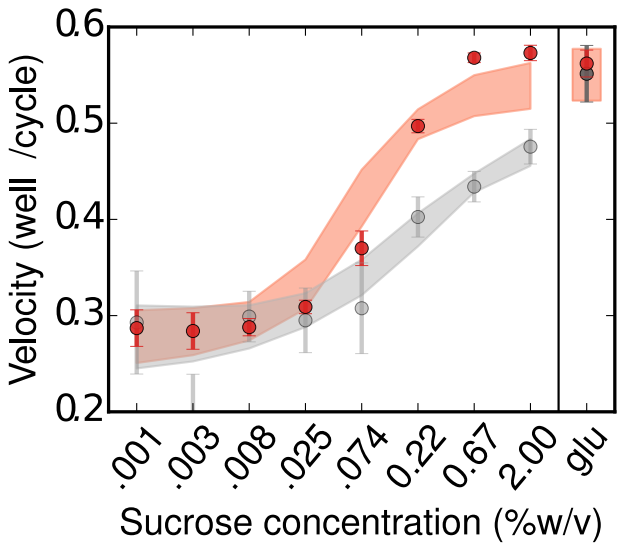

Figure S8
A mechanistic model for growth on glucose and sucrose predicts velocities close to what are observed experimentally (SI section 4)
Experimentally observed velocities in 8 different sucrose concentrations and in 0.125% glucose are shown as red points with SD errorbars. Gray points show the predicted linearized-growth velocities. Error bars are obtained by bootstrapping on the measured growth rates at low densities and calculating the linearized growth velocities. Shaded regions indicate predictions of the model. The observed velocities match well with the predictions of the model. The model also captures the transition from pulled to pushed waves as the deviation between observed and linearized-growth velocities (gray shading) around sucrose concentration of 0.025%. The width of the shaded regions is the standard deviation of simulation results for 89 parameter sets obtained by bootstrapping over the growth rate measurements and fitting the model to the bootstrapped data.

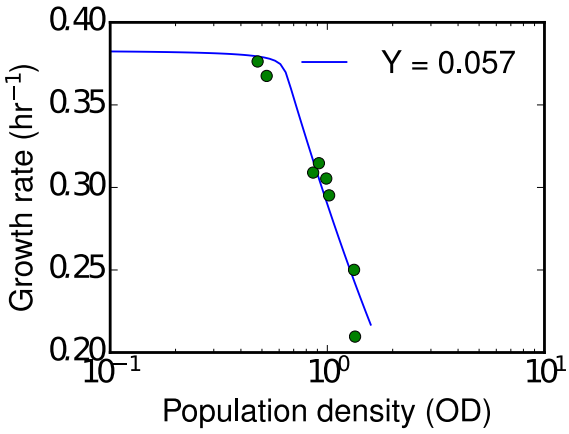

Figure S9
The yield parameter in the mechanistic model, Y, was obtained by fitting the model to growth rate measurements in 0.125% glucose, at high densities where there is a sharp decrease in growth rate with density. The yield parameter reflects the amount of glucose that a cell utilizes per division. At high cell densities, glucose is depleted quickly, causing the per capita growth rate to decrease sharply as starting OD is increased. By fitting the model to this region of growth, the value of Y can be determined accurately: Y = 0.057 OD^{-1}. Data is shown as green points, only at high densities, where growth rate is strongly affected by the yield parameter due to resource limitation.

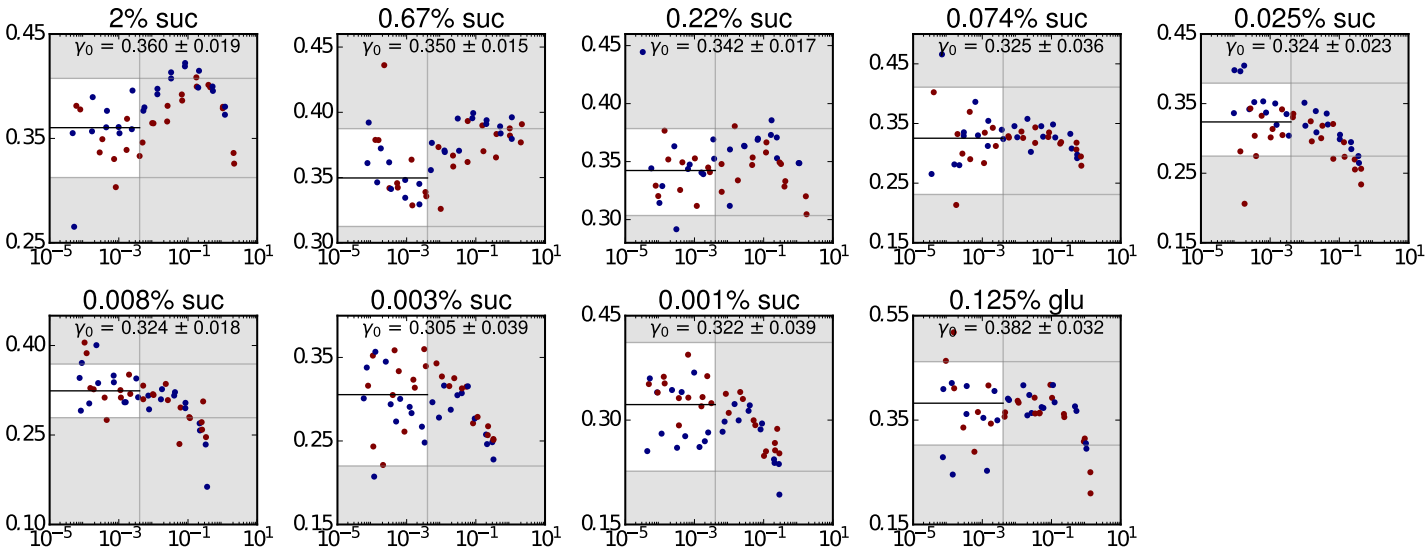

Figure S10
Low-density growth rates were measured by averaging the growth rate measurements over densities up to OD 0.004 (corresponding to 1000 cells per well). Population density is plotted along the x-axis, in terms of OD600, and growth rate is plotted along the y-axis for each panel. Data in the unshaded region is included as growth rate at low density. This region includes all data at ODs below 0.004 except for the outliers that are more than 2.5 SD away from the mean. Inset text indicates mean and S.E.M. of the unshaded data in hr^{-1}

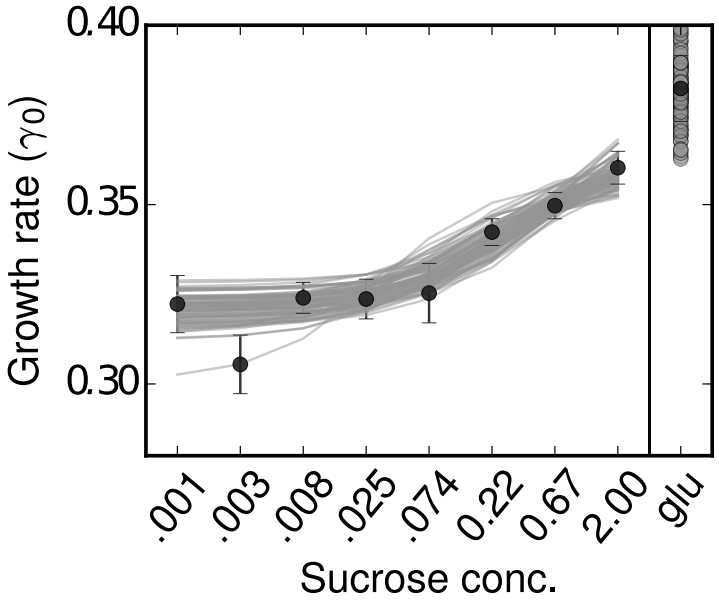

Figure S11
Low-density growth rates predicted across different sucrose concentrations by the model. We used 89 low-density parameter sets (γ_{max}, k_g, k_s, $v_s g_{eff}$) obtained by fitting to bootstrapped low-density growth rate measurements. Black circles with error bars represent the mean growth rate and s.e.m. Gray lines are model predictions. The details of the bootstrapping procedure can be found under section 4 in SI.

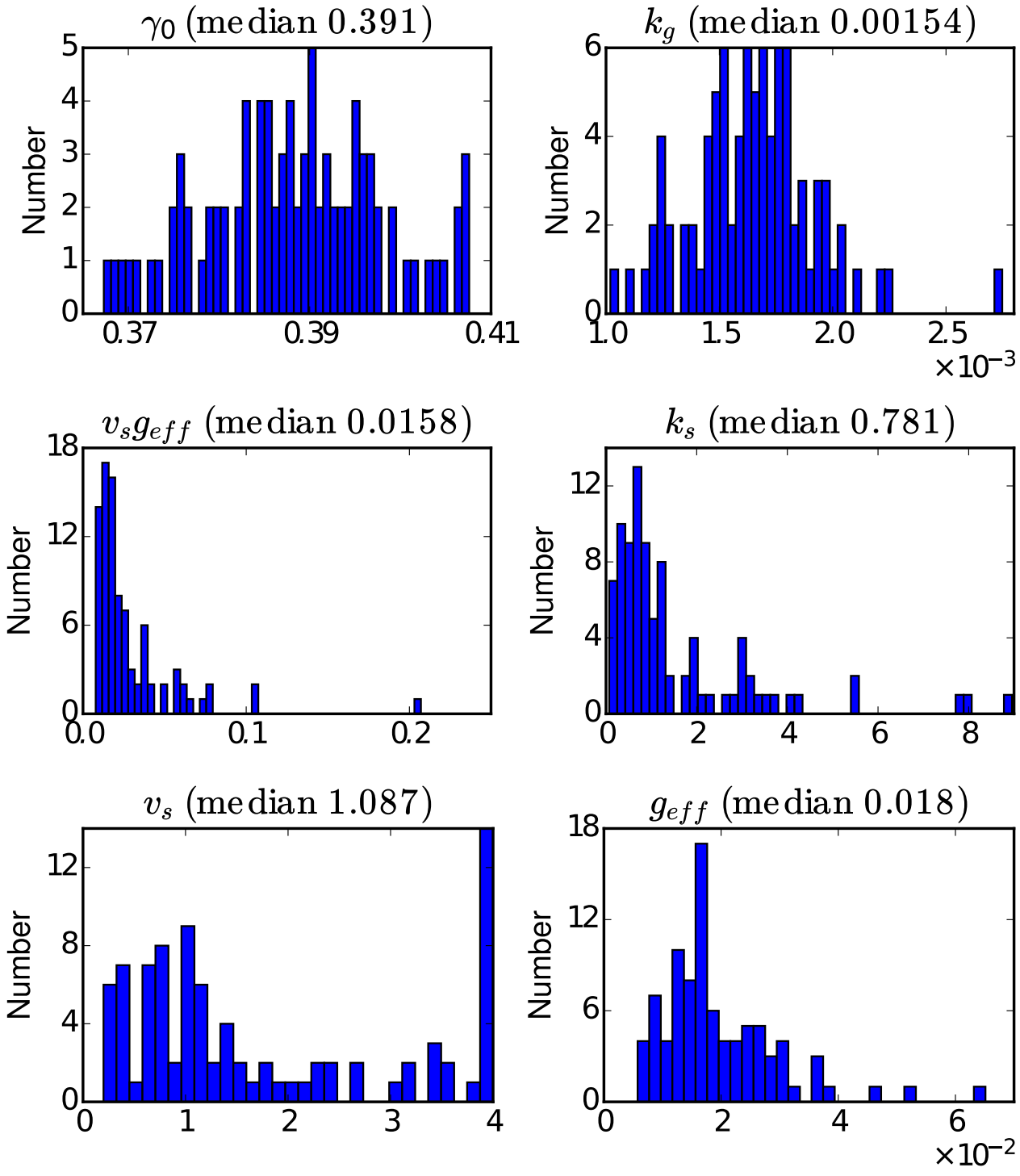

Figure S12
Distribution of parameter values in the 89 independent parameter sets obtained by bootstrapping over the data. Median values of the parameters are indicated in the title. Most median parameter values are in close agreement with previously reported values in the literature (Table S1). The exception is g_{eff}, which is expected to differ because the media is not shaken in our experiments (SI section 4).

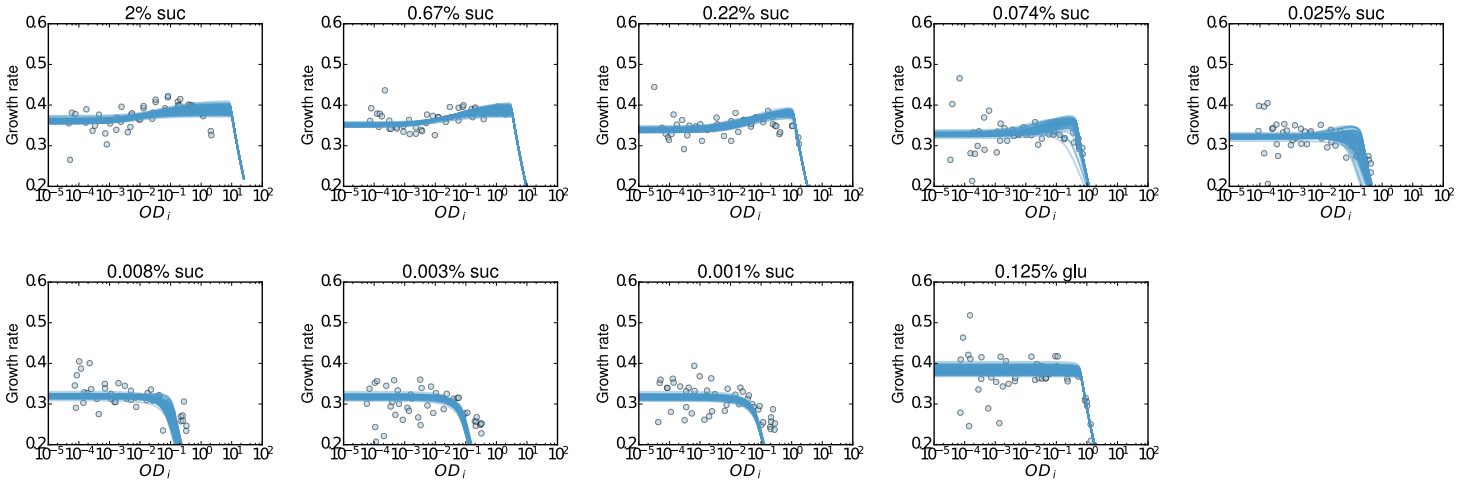

Figure S13
Allee effect increases with sucrose concentration. Measured growth rates at various cell densities are shown as blue points. Blue curves are the predictions of the model for each of the 89 parameter sets. For all parameter sets, the model matches the data well and shows an increasing Allee effect as sucrose concentration is increased.

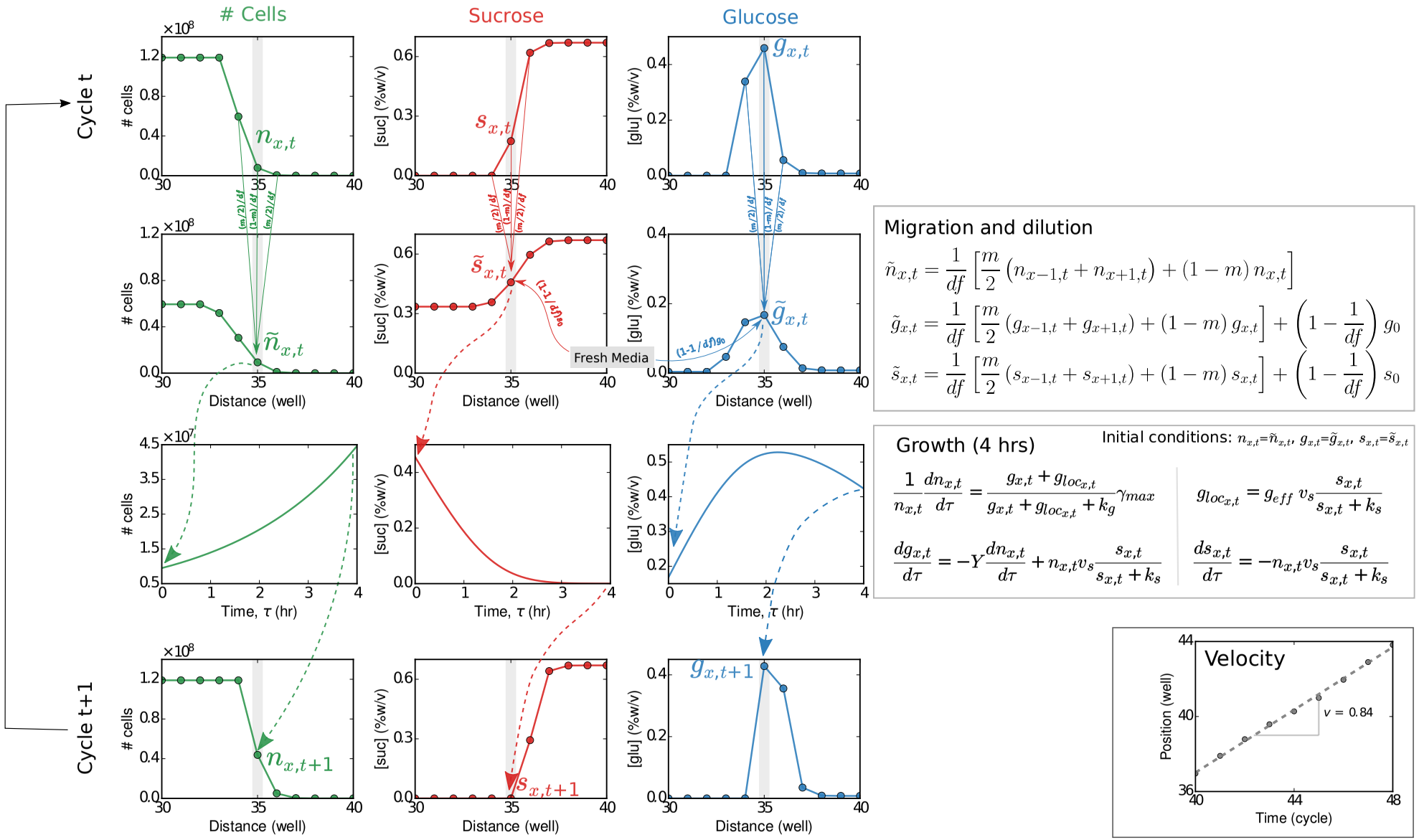

Figure S14

The figure shows how the density of cells and sugar concentrations as a function of space change over a cycle, in the simulation (SI section 5), following the dynamics in a single well highlighted above. At the end of cycle t, the cell density has a certain spatial profile (row 1). At the beginning of cycle t+1, cells are then diluted (by the factor df), and at the same time, a small fraction (m/2) is transferred to the neighbouring wells (row 2). The exact factor by which the densities change is illustrated next to the arrows from row 1 to row 2. The residual glucose and sucrose in the wells is also transferred over along with the cells. The fresh media into which the cells are diluted contains additional sugars (concentration s_0, g_0) for the cells to grow. Concentrations and cell densities at this intermediate step are denoted by $\tilde{n}$, $\tilde{g}$, $\tilde{s}$. The cells are then allowed to grow for 4 hours (row 3). In the simulations, the density at the end of 4 hours is obtained by integrating the growth model starting from the intermediate densities. Time within the growth phase is denoted by τ. The mechanistic model of growth, involving the cell densities as well as the sugar concentrations, is illustrated on the right. The profile at time t+1 is obtained at the end of growth (row 4), and the entire cycle of dilution/migration and growth is repeated. As can be seen, after the completion of a cycle, the profile is shifted in space. At a given time, t, the exact position of the wave is defined by the position at which the density profile crosses a certain threshold value (2000 cells, in the simulations). The velocity of expansion is given by the distance by which the profile shifts, averaged over multiple cycles (bottom right).

```
# Growth cycle integration
def grow(N, G, S, **kwargs):
    '''
    Takes into account the glucose and sucrose transferred over
    '''
    pars = kwargs['growth_params']
    model = kwargs['model']
    Nf, gf, sf = [], [], []
    for i in range(len(N)):
        n, g, s = N[i], G[i], S[i]
        concs = integrator(array([n, g, s]), 4, model, pars, res=0.01)[0].T
        Nf.append(concs[0][-1])
        gf.append(concs[1][-1])
        sf.append(concs[2][-1])
    return array(Nf), array(gf), array(sf)

# Final routine for each cycle
def simulate_expansion(**kwargs):
    num_cycles = kwargs['cycles']
    num_patches = len(kwargs['N_connected'])
    #dsc = kwargs['dscz']
    Npop = zeros((num_cycles, num_patches)) # Preallocate memory for the simulation
    glu, suc = ones((num_cycles, num_patches))*kwargs['g'], ones((num_cycles, num_patches))*kwargs['s']
    Npop[0] = array(kwargs['N_connected']) # Initialize the first row

    # Run simulation for num cycles
    for i in range(1, num_cycles):

        # Migrate
        Npop[i] = simulation2.discretize(simulation2.migrate(Npop[i-1], kwargs['m'], **kwargs), 1)
        df = kwargs['dilution_factor']
        m = kwargs['m']
        gSize = len(glu[i-1])
        left = arange(-1, gSize - 1) % gSize
        right = arange(1, gSize + 1) % gSize
        glu[i] = (1.-1./df)*glu[i] + 1./df*((1-m)*glu[i-1]+m/2.*(glu[i-1][left] + glu[i-1][right]))
        suc[i] = (1.-1./df)*suc[i] + 1./df*((1-m)*suc[i-1]+m/2.*(suc[i-1][left] + suc[i-1][right]))

        # Run Growth cycle
        Npop[i], glu[i], suc[i] = grow(Npop[i]/od_scale/volume, glu[i], suc[i], **kwargs)
        Npop[i] = simulation2.discretize(Npop[i]*od_scale*volume, 1)

    if 'ret_all' in kwargs.keys():
        return Npop, glu, suc
    return Npop

# Parameters
def gen_pardict(cycles=60, size=45, m=0.5, df=2, migrate='s', dilute='s', g=0.125, s=0,
                growth_pars=(0.39, 0.0019, 0.02, 0.057, 0.833, 0.781), model=jg2):
    par_dict = {
        'cycles' : cycles,
        'N_connected' : r_[zeros(size)],
        'm' : m,
        'dilution_factor' : df,
        'migrate' : migrate,
        'dilute' : dilute,
        'g' : g,
        's' : s,
        'growth_params' : growth_pars,
        'model' : model
    }
    par_dict['N_connected'][0] = 0.9
    par_dict['N_connected'][1] = 0.9
    par_dict['N_connected'][2] = 0.09
    par_dict['N_connected'][3] = 0.009
    par_dict['N_connected'][4] = 0.0009
    par_dict['N_connected'][5] = 0.00009
    par_dict['N_connected'][6] = 0.000009
    par_dict['N_connected'][7] = 0.0000009
    par_dict['N_connected'][8] = 0.00000009
    par_dict['N_connected'][9] = 0.000000009
    par_dict['N_connected'] = array(par_dict['N_connected']*od_scale*volume, int)
```

```
    return par_dict

def integrator(v_i, t, model, params, res=0.001):
    n = int(t/res)
    arr = zeros((n, len(v_i)))
    tarr = zeros(n)
    arr[0] = v_i
    for i in range(1, n):
        arr[i] = arr[i-1] + model(arr[i-1], n*res, 0, *params)*res
        arr[i][where(arr[i] < 0)] = 0
        tarr[i] = i*res
    return arr, tarr

# Growth model
def jg2(v, t, verb, gamma, kappa, geff, alpha, beta, ks):
    '''
    1. Monod growth on glucose, with some background concentration of
       glucose (preferential access to hydrolyzed sucrose/diffusion,
       now proportional to rate of sucrose hydrolysis)
    2. Glucose is absorbed at a rate proportional to the division rate
    3. Michaelis-Menten sucrose hydrolysis
    '''
    n, g, s = v
    ds = -n*beta*s/(s+ks)
    gloc = geff*beta*s/(s+ks)
    dn = n*gamma*(g+gloc)/(g+gloc+kappa)
    dg = n*beta*s/(s+ks) - alpha*dn

    if verb:
        print 'dn/dt: %.3f OD/hr, dg/dt: %.3f%%/hr, ds/dt: %.3f%%/hr, g_loc: %.4f%%'%(dn, dg, ds, gloc)

    return array([dn, dg, ds])

# Calculating velocities using a threshold
def gen_velocities(gpars, opops={}, model=jg2, thresh=2000, log_only=0):
    vvels, vlvels, vlog_par, pops = {}, {}, {}, {}
    for media in range(1, 10):
        if not log_only:
            if media not in opops.keys():
                pars = gen_pardict(g=g[media], s=s[media], growth_pars=gpars, df=10./3., m=0.5,
model=model)
                pops[media] = analyzer(simulate_expansion(**pars).T, m=0.5, df=10./3.)
            else:
                pops[media] = opops[media]
            vvels.update({media : pops[media].velocity_threshold(thresh, pops[media].times[-20:])[0]})
        else:
            pops[media] = analyzer([[],[]], m=0.5, df=10./3.)
            vvels.update({media : 0})
        vlog_par.update({media : log(comp_fold_growth([1e-7], g[media], s[media], gpars)[0][0]/1e-7)/4.})
        vlvels.update({media : pops[media].param_logistic(g=vlog_par[media])[0]})
    return vvels, vlvels, vlog_par, pops
```

References:

1. Hewitt G (2000) The genetic legacy of the Quaternary ice ages. *Nature* 405(6789):907–913.
2. Graciá E, et al. (2013) The uncertainty of Late Pleistocene range expansions in the western Mediterranean: a case study of the colonization of south-eastern Spain by the spur-thighed tortoise, Testudo graeca. *J Biogeogr* 40(2):323–334.
3. Phillips BL, Brown GP, Greenlees M, Webb JK, Shine R (2007) Rapid expansion of the cane toad (Bufo marinus) invasion front in tropical Australia. *Austral Ecol* 32(2):169–176.
4. Veit RR, Lewis MA (1996) Dispersal, Population Growth, and the Allee Effect: Dynamics of the House Finch Invasion of Eastern North America. *Am Nat* 148(2):255–274.
5. Levine JM, D'Antonio CM (2003) Forecasting Biological Invasions with Increasing International Trade. *Conserv Biol* 17(1):322–326.
6. Pateman RM, Hill JK, Roy DB, Fox R, Thomas CD (2012) Temperature-Dependent Alterations in Host Use Drive Rapid Range Expansion in a Butterfly. *Science* 336(6084):1028–1030.
7. Walther G-R, et al. (2002) Ecological responses to recent climate change. *Nature* 416(6879):389–395.
8. Pimentel D (2014) *Biological Invasions: Economic and Environmental Costs of Alien Plant, Animal, and Microbe Species* (CRC Press).
9. Mayo JH, Straka TJ, Leonard DS (2003) The Cost of Slowing the Spread of the Gypsy Moth (Lepidoptera: Lymantriidae). *J Econ Entomol* 96(5):1448–1454.
10. Johnson DM, Liebhold AM, Tobin PC, Bjørnstad ON (2006) Allee effects and pulsed invasion by the gypsy moth. *Nature* 444(7117):361–363.
11. Sutherst RW, Floyd RB, Maywald GF (1996) The Potential Geographical Distribution of the Cane Toad, Bufo marinus L. in Australia. *Conserv Biol* 10(1):294–299.
12. Leung B, Drake JM, Lodge DM (2004) Predicting invasions: propagule pressure and the gravity of allee effects. *Ecology* 85(6):1651–1660.
13. Bocedi G, et al. (2014) RangeShifter: a platform for modelling spatial eco-evolutionary dynamics and species' responses to environmental changes. *Methods Ecol Evol* 5(4):388–396.
14. Skellam JG (1951) Random Dispersal in Theoretical Populations. *Biometrika* 38(1/2):196–218.
15. Fisher RA (1937) The Wave of Advance of Advantageous Genes. *Ann Eugen* 7(4):355–369.
16. Hanski I (1999) *Metapopulation Ecology* (OUP Oxford).
17. van Saarloos W (2003) Front propagation into unstable states. *Phys Rep* 386(2–6):29–222.
18. Murray JD ed. (1993) *Mathematical Biology* (Springer-Verlag, New York).
19. Paquette GC, Chen L-Y, Goldenfeld N, Oono Y (1994) Structural stability and renormalization group for propagating fronts. *Phys Rev Lett* 72(1):76–79.
20. Courchamp F, et al. (1999) Inverse density dependence and the Allee effect. *Trends Ecol Evol* 14(10):405–410.
21. Allee WC (1949) *Principles of Animal Ecology* (Saunders Co.).

22. Kramer AM, Dennis B, Liebhold AM, Drake JM (2009) The evidence for Allee effects. *Popul Ecol* 51(3):341–354.
23. Stephens PA, Sutherland WJ, Freckleton RP (1999) What Is the Allee Effect? *Oikos* 87(1):185–190.
24. Kot M (2001) *Elements of Mathematical Ecology* (Cambridge University Press).
25. Hallatschek O, Nelson DR (2008) Gene surfing in expanding populations. *Theor Popul Biol* 73(1):158–170.
26. Korolev KS, Avlund M, Hallatschek O, Nelson DR (2010) Genetic demixing and evolution in linear stepping stone models. *Rev Mod Phys* 82(2):1691–1718.
27. Graciá E, et al. (2013) Surfing in tortoises? Empirical signs of genetic structuring owing to range expansion. *Biol Lett* 9(3):20121091.
28. Hundertmark KJ, Daele LJV (2009) Founder effect and bottleneck signatures in an introduced, insular population of elk. *Conserv Genet* 11(1):139–147.
29. Ramachandran S, et al. (2005) Support from the relationship of genetic and geographic distance in human populations for a serial founder effect originating in Africa. *Proc Natl Acad Sci U S A* 102(44):15942–15947.
30. Lewis MA, Kareiva P (1993) Allee Dynamics and the Spread of Invading Organisms. *Theor Popul Biol* 43(2):141–158.
31. Melbourne BA, Hastings A (2009) Highly Variable Spread Rates in Replicated Biological Invasions: Fundamental Limits to Predictability. *Science* 325(5947):1536–1539.
32. Wakita J, Komatsu K, Nakahara A, Matsuyama T, Matsushita M (1994) Experimental Investigation on the Validity of Population Dynamics Approach to Bacterial Colony Formation. *J Phys Soc Jpn* 63(3):1205–1211.
33. Giometto A, Rinaldo A, Carrara F, Altermatt F (2014) Emerging predictable features of replicated biological invasion fronts. *Proc Natl Acad Sci* 111(1):297–301.
34. Jessup CM, et al. (2004) Big questions, small worlds: microbial model systems in ecology. *Trends Ecol Evol* 19(4):189–197.
35. Momeni B, Brileya KA, Fields MW, Shou W (2013) Strong inter-population cooperation leads to partner intermixing in microbial communities. *eLife* 2:e00230.
36. Ben-Jacob E, et al. (1995) Complex bacterial patterns. *Nature* 373(6515):566–567.
37. Pirt SJ (1967) A Kinetic Study of the Mode of Growth of Surface Colonies of Bacteria and Fungi. *J Gen Microbiol* 47(2):181–197.
38. Korolev KS, et al. (2012) Selective sweeps in growing microbial colonies. *Phys Biol* 9(2):26008.
39. Datta MS, Korolev KS, Cvijovic I, Dudley C, Gore J (2013) Range expansion promotes cooperation in an experimental microbial metapopulation. *Proc Natl Acad Sci* 110(18):7354–7359.
40. Korolev KS (2013) The Fate of Cooperation during Range Expansions. *PLoS Comput Biol* 9(3):e1002994.

41. Chen L, et al. (2014) Two-Dimensionality of Yeast Colony Expansion Accompanied by Pattern Formation. *PLoS Comput Biol* 10(12):e1003979.
42. Van Dyken JD, Müller MJI, Mack KML, Desai MM (2013) Spatial Population Expansion Promotes the Evolution of Cooperation in an Experimental Prisoner's Dilemma. *Curr Biol* 23(10):919–923.
43. Weber MF, Poxleitner G, Hebisch E, Frey E, Opitz M (2014) Chemical warfare and survival strategies in bacterial range expansions. *J R Soc Interface* 11(96):20140172.
44. Kerr B, Riley MA, Feldman MW, Bohannan BJM (2002) Local dispersal promotes biodiversity in a real-life game of rock–paper–scissors. *Nature* 418(6894):171–174.
45. Hallatschek O, Hersen P, Ramanathan S, Nelson DR (2007) Genetic drift at expanding frontiers promotes gene segregation. *Proc Natl Acad Sci* 104(50):19926–19930.
46. Korolev KS, Xavier JB, Nelson David R, Foster KR (2011) A Quantitative Test of Population Genetics Using Spatiogenetic Patterns in Bacterial Colonies. *Am Nat* 178(4):538–552.
47. Taylor CM, Hastings A (2005) Allee effects in biological invasions. *Ecol Lett* 8(8):895–908.
48. Keitt TH, Lewis Mark A, Holt RD (2001) Allee Effects, Invasion Pinning, and Species' Borders. *Am Nat* 157(2):203–216.
49. Gore J, Youk H, van Oudenaarden A (2009) Snowdrift game dynamics and facultative cheating in yeast. *Nature* 459(7244):253–256.
50. Dai L, Vorselen D, Korolev KS, Gore J (2012) Generic Indicators for Loss of Resilience Before a Tipping Point Leading to Population Collapse. *Science* 336(6085):1175–1177.
51. Sanchez A, Gore J (2013) Feedback between Population and Evolutionary Dynamics Determines the Fate of Social Microbial Populations. *PLoS Biol* 11(4):e1001547.
52. H. Koschwanez J, R. Foster K, W. Murray A (2011) Sucrose Utilization in Budding Yeast as a Model for the Origin of Undifferentiated Multicellularity. *PLoS Biol* 9(8):e1001122.
53. Brunet É, Derrida B (2001) Effect of Microscopic Noise on Front Propagation. *J Stat Phys* 103(1–2):269–282.
54. Brunet E, Derrida B (1997) Shift in the velocity of a front due to a cutoff. *Phys Rev E* 56(3):2597–2604.
55. Kolmogorov AN, Piscounov N, Petrowski I (1937) Étude de l'équation de la diffusion avec croissance de la quantité de matière et son application a un problème biologique. *Mosc Univ Bull Math* 1:1–25.
56. Liebhold AM, Tobin PC (2006) Growth of newly established alien populations: comparison of North American gypsy moth colonies with invasion theory. *Popul Ecol* 48(4):253–262.
57. Roques L, Garnier J, Hamel F, Klein EK (2012) Allee effect promotes diversity in traveling waves of colonization. *Proc Natl Acad Sci* 109(23):8828–8833.
58. Tobin PC, Berec L, Liebhold AM (2011) Exploiting Allee effects for managing biological invasions. *Ecol Lett* 14(6):615–624.
59. Celiker H, Gore J (2012) Competition between species can stabilize public-goods cooperation within a species. *Mol Syst Biol* 8:621.

60. Bender CM, Orszag SA (1999) *Advanced Mathematical Methods for Scientists and Engineers I* (Springer New York, New York, NY) Available at: http://link.springer.com/10.1007/978-1-4757-3069-2 [Accessed October 14, 2015].
61. Mrwebi M (2004) Testing Monod : growth rate as a function of glucose concentration in Saccharomyces cerevisiae. Thesis (Stellenbosch : University of Stellenbosch). Available at: http://scholar.sun.ac.za/handle/10019.1/16398 [Accessed January 14, 2016].
62. Vitolo M, Yassuda MT (1991) Effect of sucrose concentration on the invertase activity of intact yeast cells (S. cerevisiae). *Biotechnol Lett* 13(1):53–56.
63. Goulart AJ, et al. (2013) Glucose and Fructose Production by Saccharomyces cerevisiae Invertase Immobilized on MANAE-Agarose Support. *Rev Ciênc Farm Básica E Apl* 34(2):169–175.
64. Ben-Jacob E, Brand H, Dee G, Kramer L, Langer JS (1985) Pattern propagation in nonlinear dissipative systems. *Phys Nonlinear Phenom* 14(3):348–364.